PRODUCT INHIBITION IN HUMAN MANGANESE SUPEROXIDE DISMUTASE

By

AMY S. HEARN

A DISSERTATION PRESENTED TO THE GRADUATE SCHOOL
OF THE UNIVERSITY OF FLORIDA IN PARTIAL FULFILLMENT
OF THE REQUIREMENTS FOR THE DEGREE OF
DOCTOR OF PHILOSOPHY

UNIVERSITY OF FLORIDA

2001

To the loving memory of my mother and father.
To my husband, Hunter, for all of his love and support.

ACKNOWLEDGMENTS

I would like to thank my mentor, Dr. David Silverman, for all of his guidance and support during my graduate career. He has taught me how to be a scientist and to ask the right questions. I appreciate all of the time he spent answering my questions and discussing my results. His mentorship has helped me to become an independent researcher. I would also like to thank Dr. Chingkuang Tu for all of his assistance in answering countless questions over the years. I am also grateful to the rest of the Silverman lab for all their support and helpful discussions. I would also like to express my appreciation to Kristi Totten and Dr. Ke Ren for their excellent technical assistance over my career. Lastly, I am grateful to Dr. Harry Nick for being very supportive of my project. He has always made the time to discuss my findings and showed a genuine interest in my development as a scientist.

TABLE OF CONTENTS

page

ACKNOWLEDGMENTS iii

LIST OF TABLES vii

LIST OF FIGURES viii

ABSTRACT x

CHAPTERS

1. INTRODUCTION 1

Role of Oxygen and MnSOD in Cells 1
Comparison of Superoxide Dismutases 2
Structure of MnSOD 4
Product Inhibition in MnSOD 5
Overall Research Goals 6

2. CHARACTERIZATION OF THE PRODUCT INHIBITED COMPLEX 12

Introduction 12
Materials and Methods 15
Mutagenesis and Cloning 15
Generation of MnSOD cDNA in the pTrc 99A vector 15
Preparation of Site-directed Mutants of MnSOD 16
Growth and Expression of MnSOD 17
Scanning Stopped-Flow 18
Results 19
Scanning Stopped-flow of MnSOD in Forward and Reverse Directions 19
Azide Binding to MnSOD 20
Kinetics of Decay of the Inhibited Complex 21
Discussion 22
Identification of the Product Inhibited Complex 22
Decay of the Inhibited Complex 23
Azide Binding to MnSOD 24

3. STRUCTURAL AND STABILITY STUDIES 33

Introduction 33
Materials and Methods 34
X-Ray Crystallography W161A 34
X-Ray Crystallography-W161F 35
Differential Scanning Calorimetry 36
Stopped-flow Spectrophotometry 36
Results 37
Crystal Structure-W161F 37
Crystal Structure-W161A 37
Differential Scanning Calorimetry 39
Stopped-flow Spectrophotometry 40
Discussion 40
Differential Scanning Calorimetry 40
Stopped-flow Spectrophotometry 41
X-ray Crystallography-W161F 41
X-Ray Crystallography-W161A 43

4. KINETIC STUDIES OF THE PRODUCT INHIBITED COMPLEX 52

Introduction 52
Materials and Methods 53
Preparation and Purification of Enzymes. 53
Pulse Radiolysis 55
Results 56
Observation of the Absorbance of Superoxide 56
Observation of the Absorbance of Free and Inhibited Enzyme. 58
Inhibition pH Profiles 60
Solvent Hydrogen Isotope Effects 60
Discussion 60
Kinetics of Position 161 Mutants 60
Competition Between the Inhibited and Uninhibited Pathways 61
Solvent Hydrogen Isotope Effects 62
Inhibition pH profiles 63
Application of the Simplified Mechanism 64

5. CONCLUDING REMARKS AND FUTURE DIRECTIONS 73

Conclusions 73
Future Directions 74
Site-directed Mutagenesis 74
Electron Spin Resonance 75
Redox Potential 75
EXAFS 77
Resonance Raman Spectroscopy 78
Proton Coupled Electron Transfer 78

REFERENCES 80

BIOGRAPHICAL SKETCH 85

LIST OF TABLES

Table Page

2-1: Values of the Steady-State Parameters for the Decay of Superoxide Catalyzed by Human MnSOD and Mutants 26

3-1: Transition Temperatures for the Unfolding of Wild-Type Human MnSOD and Mutants at Position 161 47

4-1: Rate Constants for the Formation (k_3) and Dissociation (k_4) of the Inhibited Complex and Their Solvent Hydrogen Isotope Effects for Human Wild-type MnSOD and Site-specific Mutants 66

4-2: Rate Constants of Eqs 4-6 and 4-7 for Catalysis by Human MnSOD and the Zero-order Rate Constant Resulting from Product Inhibition 67

LIST OF FIGURES

Figure Page

1-1: Tetrameric structure of human manganese superoxide dismutase.... 9

1-2: Close-up of the active site of human manganese superoxide dismutase..... 10

1-3: Superoxide decay catalyzed by wild-type human MnSOD as determined by pulse radiolysis. 11

2-1: Schematic of PCR reactions used to create site-directed mutants..... 27

2-2: Schematic of a sequential scanning stopped-flow spectrophotometer..... 28

2-4: Visible spectra obtained by scanning stopped-flow after mixing H_2O_2 and wild-type MnSOD. Inset: (1) The spectrum of wild-type MnSOD without the addition of H_2O_2; (2) the spectrum of wild-type MnSOD containing a 50-fold molar excess of azide ion. 30

2-5: Scanning stopped-flow spectra of (1) W161F MnSOD and (2) wild-type MnSOD both 5.2 ms after mixing with 0.95 mM $O_2^{\cdot-}$..... 31

2-6: The decay of the absorbance at 420 nm after mixing H_2O_2 and wild-type MnSOD via stopped-flow..... 32

3-1: The hydrophobic surface of human MnSOD showing the conserved hydrophobic box of residues which surround the active site. 46

3-2: Structure of the active site of W161F MnSOD (multicolored) showing the conformation of Phe161 with respect to the Mn and other active site residues from the crystal structure. Wild type structure (purple) is superimposed..... 48

3-3: Structure of the active site of human W161A MnSOD (gray) superimposed on that of wild-type human MnSOD (green) 49

3-4: Structure of the active site of wild-type human MnSOD (green) superimposed on that of W161F (pink, no sulfate used); W161F (purple, with sulfate); and W161A (gray, with sulfate). 50

3-5: The absorbance of superoxide (250 nm) vs. time in the catalyzed dismutation in the presence and absence of sulfate 51

4-1: Decrease in absorbance of superoxide at 260 nm in the presence of 1 μM W161A MnSOD measured by pulse radiolysis. 68

4-2: Increase in absorbance at 420 nm of 25 μM W161A MnSOD at short times after pulse radiolysis generated an initial concentration of 4.9 μM superoxide 69

4-3: Increase in absorbance at 480 nm of 25 μM W161A MnSOD at longer times after pulse radiolysis generated an initial concentration of 4.9 μM superoxide. Inset: Changes in absorbance at 480 nm and at 420 nm of 25 μM W161A MnSOD upon exposure to 1.7 μM superoxide. 70

4-4: The pH profile for the rate constant $k_2 + k_3$ for wild type human MnSOD and k_3 for W161A human MnSOD (eqs 4-7 and 4-8) 71

4-5: The pH profile for the rate constant k_4 (eq 4-9) for wild type human MnSOD and W161A human MnSOD 72

Abstract of Dissertation Presented to the Graduate School
of the University of Florida in Partial Fulfillment of the
Requirements for the Degree of Doctor of Philosophy

PRODUCT INHIBITION IN HUMAN MANGANESE SUPEROXIDE DISMUTASE

By

Amy S. Hearn

August 2001

Chairman: Dr. David N. Silverman
Major Department: Pharmacology and Therapeutics

Human manganese superoxide dismutase (MnSOD) is a mitochondrial redox enzyme which protects the mitochondrion from oxidative damage associated with electron transport during respiration. The enzyme catalyzes the dismutation of superoxide radicals ($O_2^{\cdot-}$) to oxygen (O_2) and hydrogen peroxide (H_2O_2). The catalysis is efficient, but the enzyme becomes inhibited within the first few milliseconds of the catalysis. This inhibition is believed to result from a complex of peroxide dianion with the manganese. The active site of MnSOD is surrounded by a series of hydrophobic residues, and the goal of this work is to better understand the role of hydrophobicity in the active site and its role in inhibition. These studies focused on Trp161, a prominent hydrophobic residue which forms one wall of the active site cavity. A series of site-directed mutants of decreasing hydrophobicity were generated at position 161, and their

properties were investigated using X-ray crystallography, differential scanning calorimetry, pulse radiolysis, and stopped-flow spectrophotometry.

The mutants at position Trp161 are the most inhibited enzymes reported for MnSOD, and X-ray crystallography showed that Trp161 is critical in orienting the residues involved in a hydrogen bonding network extending into the active site. This network is believed to supply the protons necessary for catalysis, and interruption of this hydrogen-bonding network may delay proton transfer and account for the increased inhibition observed in these mutants. Addition of product hydrogen peroxide to MnSOD observed by stopped-flow spectrophotometry showed that the inhibited complex can be generated by the addition of product. These experiments support the hypothesis of inhibition in the enzyme as a form of product inhibition. Solvent hydrogen isotope effects measured by pulse radiolysis were used to identify proton transfer steps in the catalysis. The decay of the inhibited complex was found to depend on proton transfer while its formation was found to have no rate-contributing proton transfer.

CHAPTER 1
INTRODUCTION

Role of Oxygen and MnSOD in Cells

Respiration provides many benefits to cells but also requires special defenses. This is because the stepwise reduction of oxygen generates intermediates such as superoxide, peroxide, and hydroxyl radical which can easily damage cells (Fridovich, 1986). Mitochondria utilize over 90% of the oxygen consumed in eukaryotic cells, and 1-5% of this oxygen escapes the electron transport system as oxygen radicals during respiration (Chance et al., 1979). Mitochondrial DNA is particularly vulnerable to oxygen damage resulting from the combination of the extensive oxygen metabolism within the mitochondrion, inefficient DNA repair, and lack of histones (Richter et al., 1988). Within the mitochondrion, MnSOD is of importance and interest as the primary defense against oxidative damage by converting superoxide radicals ($O_2^{\cdot-}$) to oxygen and hydrogen peroxide (Beyer et al., 1991).

Superoxide is a normal byproduct of aerobic metabolism and is produced in a variety of reactions, including photosynthesis, oxidative phosphorylation, the conversion of hypoxanthine and xanthine to uric acid during purine catabolism (Bannister et al., 1987), and the respiratory burst of activated neutrophils and macrophages (Fridovich, 1986). Damage imposed by free radical oxygen species has been connected with many degenerative processes including cancer and aging (Cerutti, 1985; Halliwell and Gutteridge, 1990; Cerutti and Trump, 1991; Homma et al., 1994). The rate of oxidative

damage to DNA has been shown to be directly proportional to metabolic rate and inversely proportional to life span (Adelman et al., 1988).

Superoxide dismutases are essential components in the physiological response to oxygen toxicity, and they are being studied as possible therapeutic agents in pathological conditions related to oxidative stress, such as post-ischemic reperfusion of organs (Murohara et al., 1991; Zweier et al., 1987), lung and tissue damage (White et al., 1991; Oda et al., 1989), acute and chronic inflammation, and ionizing radiation (Halliwell et al., 1985). Experiments by Halliwell and Guteridge (1989) support the anti-aging and anti-cancer roles for SODs. In *Drosophila*, increased SOD expression results in an increase in mean life span (Reveillaud et al., 1991). A lack of SOD in anaerobic prokaryotes is lethal upon oxygen exposure (Fridovich, 1985). Homozygous MnSOD knockout mice generated by Li and coworkers (1995) demonstrate the cellular necessity of MnSOD. The knockout mice die within 10 days of birth and exhibit various pathologies including severe dilated cardiomyopathy, metabolic acidosis, accumulation of lipid in the liver and skeletal muscle, and decreased levels of activity of the enzymes aconitase, succinate dehydrogenase, and cytochrome c oxidase. Changes in the expression levels of MnSOD have also been linked to Duchenne muscular dystrophy (Mechler et al., 1984) and Parkinson's disease (Yoritaka et al., 1997; Bostantjopoulou et al., 1997).

Comparison of Superoxide Dismutases

The superoxide dismutases are a family of metalloenzymes classified according to the metal cofactor they contain. There are four forms of SOD with different metal ions and different distributions: Cu/Zn, Fe, Mn, and Ni. The copper/zinc (Cu/Zn) SOD is not related to the highly homologous iron (Fe) and manganese (Mn) enzymes (Beyer et al., 1991). A Ni- containing SOD which is unrelated to Cu/ZnSOD, FeSOD and MnSOD's

has also been identified from *Streptomyces coelicolor* (Kim et al., 1996) and *Streptomyces seoulensis* (Choudhury et al., 1999).

The FeSOD is considered to be the most primitive because it is mainly found in anaerobic bacteria and other prokaryotes, while MnSOD is found in some prokaryotes and in the mitochondria of eukaryotic cells (Hunter et al.,1997). The Cu/Zn form of the enzyme is predominantly located in the cytoplasm of eukaryotic cells and in the chloroplasts of certain plants (Bannister et al., 1987). In vivo, the FeSOD and the Cu/Zn SOD are constitutively produced, but the MnSOD is inducible (Hassan, 1988; Touati, 1988) by paraquat (Krall et al., 1988), X-radiation (Oberley et al., 1987), hyperoxia (Housset and Junod, 1981), interleukin-1 (Masuda et al., 1988; Dougall and Nick, 1991; Visner et al., 1992; Gwinner et al., 1995), interleukin-6 (Dougall and Nick, 1991) and tumor necrosis factor (Wong et al., 1989; Visner et al., 1992)

Structural analysis of the superoxide dismutases reveals that the Fe and Mn enzymes have similar primary, secondary, and tertiary structures (Parker and Blake, 1988). These two enzymes catalyze the dismutation of superoxide at similar rates by a similar mechanism, and although the Mn and FeSOD's exhibit high sequence and structural homology, the metal activity can only be reconstituted with the metal which is present in the native enzyme. The only exceptions to this are some bacterial SOD's which are active with either iron or manganese in the active site; these SOD enzymes which do not exhibit a strict metal specificity are termed "cambialistic" SODs (Meier et al., 1994).

A possible explanation for the different specificities of the Fe and MnSODs for their metals may be due to the natural reduction midpoint potential (E^{o}) of free Fe and Mn. This could explain why the metal specific SOD's are inactive with the other metal

in the active site. Even though the two metals have similar properties in the M^{2+} and M^{3+} states, their reduction potentials for free metal are very different (0.77V for Fe and 1.51V for Mn vs. standard hydrogen electrode for the single electron reductions of free Fe^{3+} and Mn^{3+}) (Vance, 1999). Since the enzyme undergoes alternating oxidation and reduction steps in catalysis, it needs to simultaneously optimize both reactions. In order to accomplish this, the enzyme needs to adjust the E^{o} of its metal ion to approximately 0.36V, which is half way between the oxidation and reduction half reactions for the catalysis. The most likely reason for metal specificity in Fe and MnSOD's may be the differences in the natural reduction midpoint potentials between iron and manganese.

Structure of MnSOD

The crystal structure of human MnSOD has been determined to 2.2 Å resolution and has been shown to be a tetrameric dimer of dimers with one active site (containing one Mn) per 22kDa monomer (Figure 1-1) (Borgstahl et al., 1992). The metal is liganded by three histidines (26,74,163), one monodentate aspartate (159), and a single solvent molecule (see Figure 1-2) giving a distorted trigonal bipyramidal geometry (Cooper et al., 1995; Lah et al., 1995). The coordinated solvent molecule, along with Tyr34, Gln143, His30, and Tyr166, forms a hydrogen-bonding network in the active site which is thought to be important in the delivery of protons during the catalysis. Mutations have been made at Gln143 resulting in the incorporation of additional solvent molecules in the active site, a great decrease in catalytic activity, and a change in the resting redox state of the manganese to Mn^{2+} (Hsieh et al., 1998; Leveque et al., 2000). Mutations at position His30 also show a decrease in overall activity (Ramilo et al., 1999), while mutations at position Tyr34 and Tyr166 show a great increase in levels of inhibition (Guan et al. 1998; Ramilo et al., 1999).

The metal in the active site is surrounded by a hydrophobic box of mainly aromatic residues. Residues within a 7 Å radius of the metal tend to be highly conserved in all sequences, and all aromatic residues within 7 Å are totally conserved within known MnSOD sequences. This hydrophobic surface could serve several functions: ordering water in the active site, offering some electrostatic shielding, orienting important hydrogen bonds for proton transfer, or modulating the redox potential of the manganese in the active site. One of the strictly conserved residues in the hydrophobic surface is the prominent residue, Trp 161, which forms one wall of the active site cavity. This tryptophan is located 4.68 Å (γ carbon) from the manganese. Since Trp161 is located near the presumed substrate entry site, it may have an important structural or catalytic role. A goal of this work is to determine the role of this hydrophobic surface, particularly Trp161, in the enzyme by making mutations of decreasing hydrophobicity at this site.

Product Inhibition in MnSOD

MnSOD's exhibit product inhibition while the iron enzymes do not. The origin of the inhibition is believed to be a complex of peroxide dianion with the manganese. This complex is postulated to result from the isomerization of the bound peroxy ligand (O_2^{2-}) from an end-on conformation to a triangular side-on complex. This species could arise when protons are not immediately available for transfer to the product peroxide. Another possibility for the inhibition is based on the assumption that the reoxidation of Mn^{2+}SOD occurs through an outer sphere pathway through a coordinated water molecule. In this scheme, the inhibited complex arises when the hydroperoxy ligand enters the first coordination sphere of the Mn^{3+}. Proton delivery to and dissociation of such a species would occur slowly (Cabelli et al., 2000). The Fe and Mn enzymes have

similar catalytic rates and identical catalytic pathways, yet only the MnSOD exhibits this inhibited form represented below as Enz-Mn^{3+}-X (Bull et al., 1991):

$$\text{Enz-Mn}^{3+} + O_2^{\cdot -} \underset{k_{-1}}{\overset{k_1}{\leftrightarrows}} [\ \text{Enz-Mn}^{3+}\text{-}\ O_2^{\cdot -}\ ] \xrightarrow{k_2} \text{Enz-Mn}^{2+} + O_2 \qquad (1\text{-}4)$$

$$\text{Enz-Mn}^{2+} + O_2^{\cdot -} + 2H^+ \underset{k_{-3}}{\overset{k_3}{\leftrightarrows}} [\ \text{Enz-Mn}^{2+}\text{-}\ O_2^{\cdot -}\ ] + 2H^+ \xrightarrow{k_4} \text{Enz-Mn}^{3+} + H_2O_2 \qquad (1\text{-}5)$$

$$k_5 \downarrow\uparrow k_{-5}$$

$$[\ \text{Enz-Mn}^{3+}\text{-X}\ ]$$

During a complete catalytic cycle two superoxide radicals are converted to oxygen and hydrogen peroxide. Catalytic traces for the dismutation of superoxide radicals by human MnSOD via pulse radiolysis are shown in Figure 1-3. The catalytic traces of Figure 1-3 demonstrate the strong zero-order region corresponding to the presence of the inhibited complex, which accumulates within the first few milliseconds of catalysis. The zero-order rate is determined, in part, by the rate constant k_{-5} of eq 1-5 for the return of the inactive form to a species in the catalytic cycle.

Overall Research Goals

The purpose of this work was to evaluate the role of hydrophobicity, especially Trp161 in the active site and its role in product inhibition in human MnSOD. Crystal structure determinations have been used to identify structural changes and alterations in solvation within the active site upon decreasing the hydrophobicity at position 161. The crystal structures were also used to locate changes in the positions of the residues involved in the hydrogen bonding network and to make correlations with inhibition

levels. This hydrogen bonding network has been shown by previous work in our lab to be important for maximal catalysis and any changes to the network have significant structural and/or catalytic effects. Differential scanning calorimetry was also utilized to evaluate the role of Trp161 in the thermostability of the enzyme.

Another question addressed in this work was whether the enzyme can be forced to work in the reverse direction by the addition of product hydrogen peroxide via stopped-flow, and if the spectrum of the enzyme upon the addition of product was the same as the enzyme in the inhibited form. I also investigated the structure of the inhibited complex by comparing product inhibition and azide binding. Correlations were made with previous work from other labs on the product inhibited form and azide bound forms of the enzyme (Bull et al., 1991; Lah et al., 1995). A relationship between the zero-order inhibited region and product inhibition has also been established. I have also determined where on the mechanistic pathway the inhibited complex arises.

A further goal was to better understand the mechanism of inhibition and to pinpoint the proton transfer steps of the catalysis using pulse radiolysis and stopped-flow techniques. pH profiles for the rate constants associated with inhibition have also been determined. Solvent hydrogen isotope effect experiments were used to determine whether the formation and decay of the product inhibited complex were proton transfer dependent. With pulse radiolysis, the individual rate constants of the mutants at position W161 and several other sites were determined to discover the relationship between the inhibited and uninhibited pathways of catalysis and proton availability. The ultimate goal of this work is to better understand inhibition in the enzyme with insights into how to free the enzyme from this catalytic inefficiency. One important feature to bear in mind is that MnSOD may have been selected for over FeSOD in eukaryotic cells in order to limit the

production of hydrogen peroxide, which is also toxic to cells. The expression of MnSOD needs to be in balance with the expression of catalase and glutathione peroxidase which break down hydrogen peroxide. Through the use of Mn as the metal cofactor, the level of activity of MnSOD in the cell may be controlled.

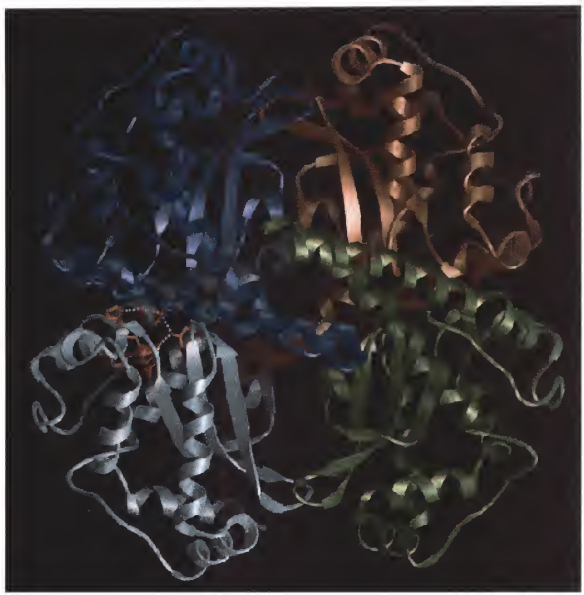

Figure 1-1: Tetrameric structure of human manganese superoxide dismutase from Borgstahl et al. (1992) with each 22 kD subunit shown in a different color. The ligands are included in the gray subunit.

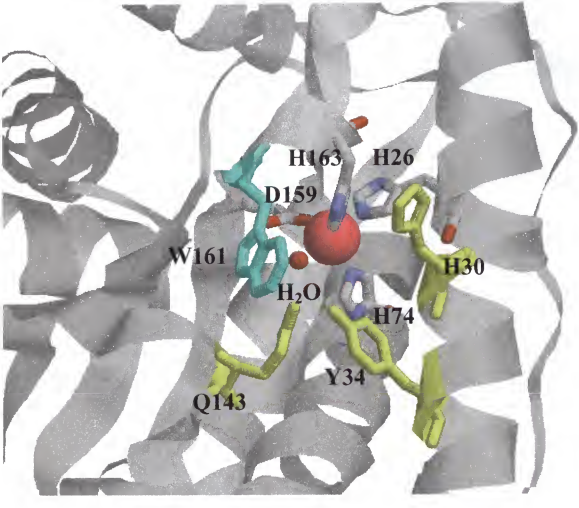

Figure 1-2: Close-up of the active site of human manganese superoxide dismutase (MnSOD). The manganese ion is shown in space-filling conformation (pink). The ligands to the manganese are shown in CPK color scheme (carbon: gray, oxygen: red, and nitrogen: light blue). Prominent residues involved in the hydrogen bonding network within the active site are shown in yellow. The important hydrophobic residue Trp161 is shown in cyan.

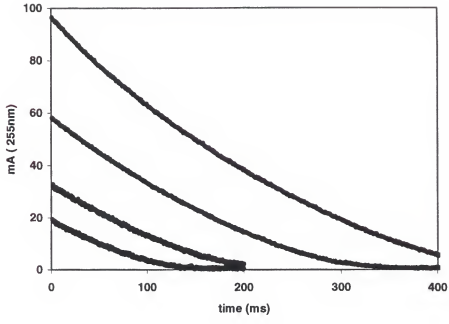

Figure 1-3: Superoxide decay catalyzed by wild-type human MnSOD as determined by pulse radiolysis. The traces show the decay of superoxide at 255 nm ($\varepsilon = 2000\ M^{-1}cm^{-1}$) versus time in milliseconds. All solutions contained 0.5 μM enzyme, 2 mM TAPS buffer, 30 mM sodium formate (as a hydroxyl radical scavenger), 50 μM EDTA (to chelate any extraneous metals in solution), at pH 8.2. Traces from the top of the figure correspond to 23.9, 14.2, 8.0. and 4.7 μM superoxide.

CHAPTER 2
CHARACTERIZATION OF THE PRODUCT INHIBITED COMPLEX

Introduction

Initial studies of MnSOD from *Bacillus stearothermophilus* used pulse radiolysis to determine that there is an initial burst of activity followed by an extended region of zero-order decay of superoxide. The zero-order region was explained as due to the presence of a reversibly inhibited form of the enzyme that can interconvert to an active form (McAdam et al., 1977). Bull et al. (1991) observed the visible absorption spectrum of the enzyme during the zero-order phase of catalysis and, on the basis of comparison to visible absorption spectra of inorganic complexes, suggested that the zero-order phase results from product inhibition by peroxide. More specifically, they suggested a side-on peroxo complex of Mn^{3+}SOD resulting from the oxidative addition of $O_2^{\cdot-}$ to Mn^{2+}SOD. This scheme is based on inorganic complexes of Mn^{3+} and peroxide in which peroxide binds in a side-on manner (Lever and Gray, 1978):

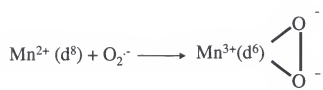

(2-1)

Another possibility is that inhibition occurs by the conversion of an outer to an inner sphere complex of product peroxide with the manganese. This complex could

result from the direct inner sphere coordination of the peroxide dianion to the metal to form the inhibited complex from which protonation and dissociation of product hydrogen peroxide occurs very slowly, whereas on the uninhibited pathway the reoxidation of Mn^{2+}SOD could occur via an outer sphere pathway through the coordinated solvent molecule. With an inner sphere coordination of Mn^{2+} and peroxide dianion, the delivery of protons may not be optimized giving rise to the inhibited form of the enzyme (Cabelli et al., 2000).

Both Cu/ZnSOD and FeSOD are irreversibly inactivated by hydroxyl radicals produced by the Fenton reactions of H_2O_2 with their metal ions (Cabelli et al., 2000); MnSOD is not irreversibly inactivated in this manner. Thus, product inhibition for MnSOD refers to the transitory inhibited complex of the zero-order phase observed during catalysis by MnSOD, and not to the irreversible type of inactivation that occurs in FeSOD and Cu/ZnSOD.

Tyr 34, a conserved residue in MnSOD and FeSOD, is part of an extensive hydrogen bond network that includes Gln 143 and the metal-ligand cluster, and this network may connect the properties of this tyrosine to catalysis at the metal (Borgstahl et al., 1992; Sorkin et al., 1997). The crystal structure of Y34F MnSOD shows that its active-site is nearly superimposable with that of the wild type except for the absence of the side-chain hydroxyl of residue 34 (Guan et al., 1998). The mutants Y34F MnSOD and Y34F FeSOD have been utilized in a number of studies comparing their catalytic and spectral properties to the wild type (Sorkin et al., 1997; Guan et al., 1998; Hunter et al., 1997; Whittaker and Whittaker, 1997). The catalytic activity of these mutants is decreased as much as 10-fold. Y34F MnSOD is more product inhibited during catalysis

than wild type, demonstrated by the smaller decrease in $[O_2^{\cdot-}]$ during the initial burst of catalysis and by a four-fold slower rate in the zero-order inhibited region for Y34F compared with wild type (Table 2-1) (Guan et al., 1998).

Another prominent residue is Trp 161 which forms one side of the active-site cavity with the manganese adjacent to the plane of its aromatic ring and 5.6 Å from the Nε of the indole ring. The crystal structure of the wild type shows the manganese-bound aqueous ligand extending into the active-site cavity with the metal-oxygen bond pointing directly toward the side chain of Trp 161 and with its oxygen 4.0 Å from the Nε of the indole ring (Borgstahl et al., 1992). The conservative mutation W161F was prepared, and this mutant was found to be the most inhibited mutant reported for human MnSOD (Table 2-1) (see Chapter 3 for structure and Chapter 4 for kinetics).

Scanning stopped-flow spectrophotometry was used to measure both the appearance of the inhibited enzyme in the zero-order phase of the dismutation of $O_2^{\cdot-}$ catalyzed by MnSOD and the reduction of Mn^{3+}SOD by excess H_2O_2; these measurements were extended to Y34F and W161F MnSOD as well. In all experiments, the absorbance of the enzyme in the visible region was followed. An intermediate in the reduction by H_2O_2 was observed that has a visible spectrum nearly identical to that for the inhibited enzyme during the zero-order phase of catalysis of superoxide dismutation. This observation confirms the suggestion that the zero-order phase during catalysis represents a product inhibited enzyme rather than alternative explanations such as a conformational change involving an inactive state.

Materials and Methods

Mutagenesis and Cloning

Generation of MnSOD cDNA in the pTrc 99A vector

The plasmid phMnSOD4 (ATCC #59947) contained the complete 222 amino acid precursor MnSOD cDNA and also a short 5' and 3' untranslated region. The first 24 amino acids of the gene make up the signal peptide which targets the protein to the mitochondrion. This signal peptide is cleaved in the mitochondrion to yield a mature 198 amino acid protein. For expression in *E. coli*, the cDNA encoding the 198 amino acids of the active enzyme plus the 3' untranslated region was amplified using the polymerase chain reaction (PCR). The DNA template for this reaction was the phMnSOD4 clone, and the primers used for the reaction were primer 1: 5'-C GCT AGT AAT CAT TTC ATG AAG CAC AGC CTC CCC G-3' and primer 2: 5'-GCA GCT TAC TGT ATT CTG CAG-3'. The first primer contains a *Bsp*H I restriction site which precedes the sequence coding for the amino terminus of the protein. The second primer is identical to the 21 base pair 3' untranslated region. The resulting PCR product was ligated into the expression vector pTrc 99A. The PCR reaction contained the following: 2 ng cDNA template, 1.5 mM $MgCl_2$, 1 mM primers 1 and 2, 250 mM dNTP's, PCR buffer, 1 unit vent polymerase, and distilled water to a final volume of 100 µL. An ERICOM thermocycler was run for 25 cycles with a 65 ^{o}C annealing temperature. The resulting PCR product was purified by electroelution, then digested with *Bsp*H I and *Pst* I and then ligated to the pre-cut pTrc 99A expression vector. The vector was pre-cut with *Nco* I and *Pst* I. *Nco* I has compatible ends with *Bsp*H I. The resulting vector was used to make all site-directed mutants of hMnSOD.

Preparation of Site-directed Mutants of MnSOD

Turbo-PFU polymerase (New England Biolabs) was used to catalyze the PCR reactions. Four primers were used to generate the mutants W161F and Y34F. The first pair of oligonucleotides was the same for a both of the mutants and was used to regenerate the entire coding region: primer 1: 5' C GCT AGT AAT CAT TTC ATG AAG CAC AGC CTC CCC G-3' and primer 2: 5'-CGC CAA AAC AGC CAA GCT TTC ATG CTC GCA G-3'. The second pair of oligonucleotides (designated primers 3 and 4) were complementary internal primers which encoded the mutation of interest (underlined). The primers used were as follows: W161F primer 3: 5'-GGG ATT GAT GTG TTC GAG CAT GCT TAC-3' and primer 4: 5'-GTA AGC ATG CTC GAA CAC ATC AAT CCC-3', Y34F primer 3: 5'-C CAC GCG GCC TTC GTT AAC AAC CTG-3', and primer 4: 5'-CAG GTT GTT AAC GAA GGC CGC CGT GG-3'. The 5' half of the coding sequence was amplified using primers 1 and 4, while a second reaction using primers 2 and 3 generated the 3' half of the MnSOD coding sequence (see Figure 2-1). A second round of PCR was performed using the products from the first two reactions (purified by electroelution) as templates with primers 1 and 2. The restriction sites *Bsp*H I and *Pst* I (incorporated into primers 1 and 2, respectively) were used for cloning the PCR products into the expression vector pTrc 99A (Pharmacia Corp.). The *Bsp*H I site, which is located in the N-terminal portion of the protein, was annealed to the compatible cohesive ends of the *Nco* I site in pTrc 99A, regenerating an ATG codon. *Pst* I was used to cut and anneal the C-terminal end of the cDNA to pTrc 99A. The plasmid was then transformed into the null mutant *Sod A*$^{-}$*/Sod B*$^{-}$ *E. coli* (strain QC774) (Carlioz and Touati, 1986), where it expressed human MnSOD as a mature protein tagged with an extra methionine at the amino terminus. Colonies were screened by restriction digestion with *Pst* I and with the

internal cut of *Sph* I. A small scale protein production was performed on positive clones, and a clone with appropriate levels of expression was sent to the DNA sequencing lab to verify the coding sequence including the new mutation. The top and bottom strands were sequenced to ensure accuracy. Following sequencing, the mutant was kept as a glycerol stock in the *E. coli* QC774 cells at –80 °C, and the plasmid was stored in TE buffer at -20 °C .

Growth and Expression of MnSOD

In order to express the mutant MnSOD, thirteen liters of *E. coli* (QC774) were grown to an OD_{600} = 0.4 in 2 x YT media which contains tryptone and yeast extract. At this OD, the cells were induced with 0.2 mM IPTG and 660 μM $MnCl_2$ and grown an additional 4 hours. The cells were then collected by centrifugation, and the resulting bacterial cell pellets were frozen overnight at –80 °C.

Mutant human MnSOD enzymes were purified from *E. coli* (QC774) according to the procedures of Beck et al. (1988). The cell pellet was thawed at room temperature and resuspended in 200 mL of lysis buffer which contained the following: 50 mM KH_2PO_4, pH 7.8, 25 mL glycerol, 0.2 mg/mL lysozyme, 10 μg/mL DNAse I, 0.1 mM EDTA, and 400 μL/ 200 mL Triton x100 detergent. The cells were stirred at room temperature for 2 hours, then heated to 60 °C for 45 minutes. The lysate was then centrifuged at 18,000 rpm for 20 minutes. The resulting supernatant was then placed in dialysis tubing (MW cutoff 30kD) and dialyzed three times for 24 hours against 4 liters of 2 mM KH_2PO_4 with 1 mM EDTA. The sample was then loaded onto the pre-equilibrated anion exchange column, DE-52 (Whatman), and eluted with 20 mM KH_2PO_4. The fractions containing protein (based on A_{280}) were then combined and concentrated, and the buffer (20 mM KH_2PO_4) was then replaced with 20 mM potassium acetate, pH 5.5, by repeated ultrafiltration and

addition of the new buffer. The resulting sample (30 mL) was then loaded on the cation exchanging column, CM-52 (Whatman), which was pre-equilibrated with 20 mM potassium acetate. Following loading, the column was washed with an additional 250 mL of 20 mM potassium acetate, pH 5.5, after which a gradient of 20 mM and 200 mM potassium acetate, pH 5.5 was started. SDS-polyacrylamide gels were used to visualize the final purity of the resulting fractions. The gels showed one intense band around 22 kDa, indicative of the monomer. The fractions containing protein were then concentrated via ultrafiltration, and the buffer was changed back to 20 mM KH_2PO_4 through the repeated concentration and addition of the appropriate buffer. Yields of human MnSOD mutant protein were approximately 70 mg protein per 50g of bacterial pellet. Following concentration to a few mL, the enzyme was passed through a 22 μm filter for sterilization. The sterile enzyme was stored at 4 °C.

Following extensive dialysis, the metal content of each of the samples was determined by atomic absorption spectroscopy. The manganese concentration was used in all of our calculations as the concentration of active enzyme. Protein concentrations were determined by the Lowry method; the ratio of manganese concentration to total protein concentration for Y34F and W161F was approximately 0.80.

Scanning Stopped-Flow

Properties of the enzyme in its reaction with product hydrogen peroxide were monitored by observation of the visible absorption spectrum of wild-type and Y34F MnSOD using a rapid scanning stopped-flow spectrophotometer (On-Line Instrument Systems, Inc., Bogart, Georgia or Applied Photophysics, Ltd. SX.18MV). One syringe contained a buffered solution of human MnSOD and a second syringe contained a

buffered solution of H_2O_2; final concentrations after mixing are given in the figure legends.

The visible spectra of wild-type MnSOD, Y34F, and W161F MnSOD during catalysis of the decay of $O_2^{\cdot-}$ were observed by scanning stopped-flow spectrophotometry (Applied Photophysics Ltd., SX.18MV) (schematic shown in Figure 2-2) in which KO_2 in a solution of dimethylsulfoxide and 18-crown-6 (added to increase solubility of KO_2) (Valentine and Curtis., 1975; McClune and Fee, 1978) was diluted in a sequential mixing experiment. To attain a sufficiently large final concentration of $O_2^{\cdot-}$, this initial solution of KO_2 was not greatly diluted; in the first mixing the solution containing KO_2 was diluted 1:3.5 with 2 mM Caps and 1 mM EDTA at pH 11. This solution was allowed to age 1 s before the second mixing which was 1:1 with the buffered enzyme solution. The final concentrations after mixing are given in the figure legends. Superoxide solutions were made fresh daily and stored in a dessicator prior to use.

Results

Scanning Stopped-flow of MnSOD in Forward and Reverse Directions

Using scanning stopped-flow spectrophotometry and mixing $O_2^{\cdot-}$ with Y34F MnSOD, and in separate experiments mixing H_2O_2 with Y34F MnSOD, I observed similar spectra characterized by an absorption with a maximum at 420 nm (Figure 2-3). The same experiments mixing H_2O_2 and wild-type MnSOD also showed similar spectra with maximum at 420 nm and a weak absorption near 630 nm (Figure 2-4); the spectrum for mixing $O_2^{\cdot-}$ and wild-type MnSOD also showed an absorption at 420 nm but of lesser intensity compared to W161F (Figure 2-5). It is interesting that the two most inhibited mutants of MnSOD studied show a greater intensity of the 420 nm absorbance than the

wild-type. These spectra are very similar to that of the complex which characterizes the zero-order phase in the $O_2^{\cdot-}$, dismutation direction measured by Bull et al. (1991) for *Thermus thermophilus* MnSOD which has a maximum at 410 nm and a weak band at 650 nm. Moreover, the extinction coefficient at 420 nm for the complex derived from the spectrum of human MnSOD after mixing with H_2O_2 (Figure 2-4) is 500 $M^{-1}cm^{-1}$, assuming complete conversion of enzyme to inhibited complex. This is an underestimate because it neglects the intermediate lost during the dead time of the instrument (~1.4 ms). The value of ε_{410} = 700 $M^{-1}cm^{-1}$ was found for this complex by Bull et al. (1991) measuring catalysis in the forward dismutation direction.

The visible absorption spectrum of wild-type human Mn^{3+}SOD is dominated by a broad peak with a maximum at 480 nm (ε_{480} = 600 $M^{-1}cm^{-1}$) (Figure 2-4, inset curve 1); this is the predominant redox form of purified MnSOD (Bull et al., 1991). The reduced enzyme Mn^{2+}SOD has an absorption spectrum that is very weak with broad absorption (ε < 50 $M^{-1}cm^{-1}$) and no peak in the range of 450 to 600 nm (Bull et al., 1991; Fee et al., 1976).

Azide Binding to MnSOD

The binding of azide to the wild-type human MnSOD was also investigated. The ratio of azide to enzyme concentrations was varied from 1:1 to 200:1. Interestingly, the spectrum of the enzyme fully complexed with azide (Figure 2-4, inset curve 2) closely resembled that of the enzyme in the presence of excess hydrogen peroxide (Figures 2-3, 2-4), both showing a maximum absorbance near 420 nm.

Kinetics of Decay of the Inhibited Complex

Since it took large concentrations of H_2O_2 to observe the spectra of the inhibited complex, their rate of appearance was too rapid to be measured within the dead time of the stopped-flow. However, I did observe the disappearance of these spectra to a very weak absorption consistent with the formation of Mn^{2+}SOD (Figures 2-4, 2-6). The decrease of the absorption at 420 nm was adequately fit by a process second order in wild-type enzyme with a rate constant of 55.5 ± 0.5 (absorbance units)$^{-1}$s^{-1} (Figure 2-6). This corresponds to a rate constant of 0.1 $M^{-1}s^{-1}$ assuming ε_{420} = 500 $M^{-1}cm^{-1}$ for the complex. This result is similar to the value of 40 (absorbance units) $^{-1}s^{-1}$ obtained from the experiment of Bull et al. (1991) observing the decay at 480 nm after the introduction of H_2O_2 to wild-type MnSOD. The decrease of the absorption at 420 nm (Figure 2-6) appeared equally well fit by the sum of two first-order processes with rate constants 7.0 ± 0.1 s^{-1} and 0.66 ± 0.01 s^{-1} .

The disappearance of the 420 nm absorption peak after mixing H_2O_2 with Y34F MnSOD was also observed. The second-order rate constant for decrease of the maximum at 420 nm was 23.7 ± 0.2 (absorbance units) $^{-1}$ s^{-1}. When fit to the sum of two exponentials, the rate constants were 4.1 ± 0.1 s^{-1} and 0.47 ± 0.01 s^{-1}.

In parallel experiments, human MnSOD was exposed briefly (ten seconds) to 100-fold molar excess of H_2O_2 which was then rapidly diluted. Subsequent removal of H_2O_2 by dialysis resulted in MnSOD that was fully active as measured by stopped-flow. Unlike its analog FeSOD which is inactivated in the presence of H_2O_2 through the Fenton-type chemistry in which H_2O_2 reacts with iron (Fridovich, 1986), MnSOD is not a redox catalyst for Fenton chemistry. The result that MnSOD is not irreversibly inactivated with

H_2O_2 is consistent with earlier reports of McAdam et al. (1977) and more recent studies of Yamakura et al. (1998).

An estimate of the enhanced product inhibition of the mutant W161F MnSOD was obtained by scanning stopped-flow spectrophotometry. Under comparable conditions in a scanning stopped-flow experiment, W161F MnSOD showed much stronger evidence than wild type for the presence of the inhibited state, as indicated by the larger absorbance at 420 nm (Figure 2-5). These data are consistent with the enhanced inhibited phase of catalysis in W161F compared with wild-type MnSOD observed by pulse radiolysis (Cabelli et al., 1999).

Discussion

Identification of the Product Inhibited Complex

The rapid mixing of H_2O_2 with human Mn^{3+}SOD and subsequent scanning stopped-flow spectrophotometry has resulted in the appearance of a visible absorption spectrum (Figure 2-4) with a maximum and extinction coefficient very similar to that obtained by Bull et al. (1991) for the inhibited complex in the dismutation direction, obtained after mixing of $O_2^{\cdot-}$ and *Thermus thermophilus* MnSOD. Moreover, the spectra of Figure 2-4 are also similar to the spectrum of the inhibited complex of Y34F MnSOD in the dismutation direction and, in a separate experiment in the reverse direction, after mixing with H_2O_2 (Figure 2-3). The spectrum of W161F in the $O_2^{\cdot-}$ dismutation direction also reveals a strong absorbance at 420 nm while that of the wild-type shows less intensity under the same conditions (Figure 2-5). Each spectrum shows a predominant absorbance near 420 nm and often a weak absorbance near 630 nm. This is the first reported observation of this complex obtained by the opposing reaction of H_2O_2

with MnSOD. It is significant in showing the nature of the zero-order phase of catalysis, supporting the interpretation of this phase as a form of product inhibition and providing another means by which this inhibition can be investigated. This result renders much less likely the attribution of this zero-order phase to a conformational change not related to product binding.

Decay of the Inhibited Complex

At the rather large concentrations of both H_2O_2 and Mn^{3+}SOD that were used, I did not observe the build up of the concentration of the intermediate which must occur within the dead time (near 1.4 ms) of the instrument. Instead, I have observed the decay of this intermediate complex to the featureless visible spectrum characteristic of Mn^{2+}SOD (Figure 2-4). The decrease of the absorption at 420 nm characteristic of the intermediate form (Figure 2-6) was adequately fit either by a process second order in enzyme or by the sum of two exponentials. It is unclear whether the second-order or the sum of two first-order processes is the best representation of the reaction. The larger of the first-order rate constants, 7 s^{-1}, is close to $k_{-5} = 10\ s^{-1}$ determined by Bull et al. (1991) by fitting progress curves (2 °C) of the dismutation catalysis, although it is smaller than the value of 130 s^{-1} (20 °C) determined for k_{-5} by Hsu et al. (1996). The slower rate constant of these two exponentials, 0.7 s^{-1}, is less readily explicable but could describe a long-lived intermediate in the decay of Enz-Mn^{3+}-X (Eq 1-5) or one of the many reactivities of $O_2^{\cdot-}$ and H_2O_2 (Sawyer and Valentine, 1981). Bull et al. (1991) carried out experiments observing the rate of decrease of the absorbance at 480 nm following mixing by stopped-flow of *T. thermophilus* MnSOD and excess H_2O_2. The decay of the 480 nm absorbance was best fit by second-order kinetics which they ascribe to the slow reduction of Mn^{3+}SOD by H_2O_2 resulting in Mn^{2+}SOD and $O_2^{\cdot-}$, and then the subsequent reaction of

$O_2^{\cdot-}$ with a second Mn^{3+}SOD. The work reported here differs in that it addresses the 420 nm absorption characteristic of the inhibited form of the enzyme.

Regardless of whether the decay of the peroxide-enzyme complex is best described by a second-order or two first-order processes, it was observed that the visible absorption spectrum of the intermediate formed upon mixing H_2O_2 and Mn^{3+}SOD changed to that consistent with Mn^{2+}SOD about twice as fast for wild type as for Y34F MnSOD. This smaller rate of decay of the inhibited complex for Y34F MnSOD probably contributes to the enhanced product inhibition of this mutant compared with wild type. The models for catalysis of both McAdam et al. (1977) and Bull et al. (1991) relate the magnitude of inhibition and the zero-order rate constant of the inhibited phase to this decay rate designated k_{-5} of eq 1-5. However, it is important to point out that many of the rate constants of Eqs. 1-4 and 1-5 besides k_{-5} could also possibly contribute to the greater product inhibition of Y34F MnSOD observed during the catalyzed dismutation of $O_2^{\cdot-}$; the observation of a smaller rate of decay for the spectrum of the complex formed on mixing H_2O_2 and Y34F MnSOD is suggestive rather than sufficient for greater product inhibition in the dismutation direction.

Azide Binding to MnSOD

I observed a similarity in visible absorption spectra of MnSOD in the presence of excess hydrogen peroxide and MnSOD complexed with azide (Figure 2-4, inset curve 2). The crystal structure of the azide complex of Mn^{3+}SOD from *Thermus thermophilus* shows a six-coordinate species with the azide bound to the metal and forming a hydrogen bond with the hydroxyl of Tyr 34 (Lah et al., 1995). This suggests that the complex I observed in the presence of hydrogen peroxide, like the azide complex, may have expanded coordination geometry which might occur if the peroxide is a direct ligand in

its complex with Mn^{3+}SOD and does not displace the bound water, or the peroxy ligand displaces the bound water by forming a side-on peroxo (bidentate) complex as proposed by Bull et al. (1991).

Table 2-1: Values of the Steady-State Parameters for the Decay of Superoxide Catalyzed by Human MnSOD and Mutants

enzyme	k_{cat} (s^{-1})	k_{cat}/K_m ($\mu M^{-1}s^{-1}$)	$k_o/[E_o]$ (s^{-1})
wild type[a]	40,000	800	500
Y34F[a]	3,300	870	80
W161F[b]	> 1000[c]	250	50

[a]pH 9.4 and 20°C from Guan et al. (1998)
[b]pH 9.2 and 25°C
[c]Km is large for this mutant and with pulse radiolysis we were not able to increase superoxide to values large enough to measure k_{cat}.

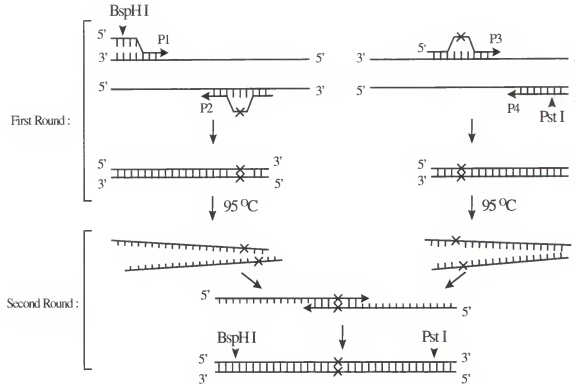

Figure 2-1: Schematic of PCR reactions used to create site-directed mutants. The first round corresponds to the first two PCR reactions used to generate each half of the gene. These fragments are used as the templates in the second round of PCR. P1, P2, P3, and P4 correspond to each of the four primers used for the reaction. P2 and P3 are internal primers containing the mutation of interest.

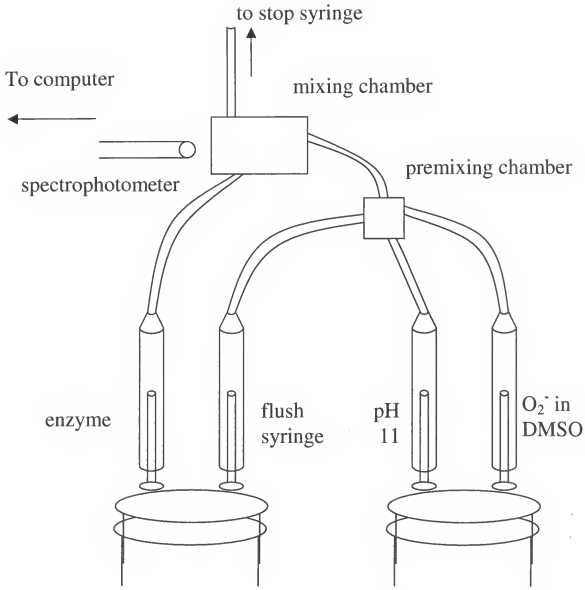

Figure 2-2: Schematic of a sequential scanning stopped-flow spectrophotometer. The initial premix occurs in the premixing chamber between the pH 11 buffer and $O_2^{\cdot}$ in DMSO solutions. Following a 1 s delay the second mixing step occurs between the contents of the premixing chamber and the enzyme solution. Pneumatic drives push the contents of the syringes into the mixing chambers.

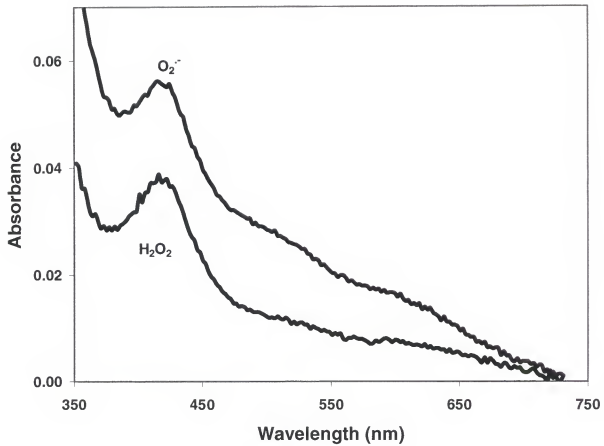

Figure 2-3: Visible spectrum obtained by scanning stopped-flow at 44 ms after mixing $O_2^{\cdot-}$ and Y34F MnSOD (top), and visible spectrum at 44 ms after mixing H_2O_2 and Y34F MnSOD (bottom). Following mixing, solutions contained 0.25 mM Y34F MnSOD, 100 mM CHES, 1.0 mM EDTA at pH 9.1 and 20 °C. The final solution for the $O_2^{\cdot-}$ catalysis contained in addition 1.0 mM CAPS and 14% dimethyl sulfoxide by volume. Initial concentration of $O_2^{\cdot-}$ was 1.0 mM; initial concentration of H_2O_2 was 25 mM.

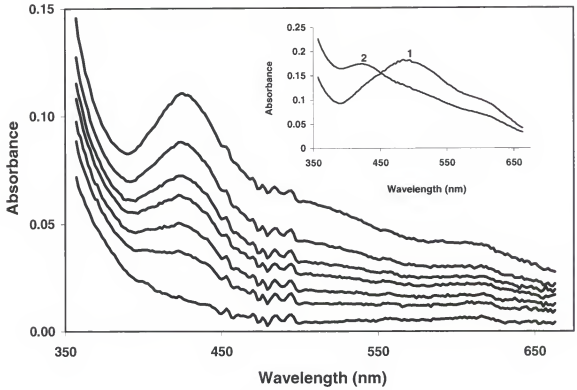

Figure 2-4: Visible spectra obtained by scanning stopped-flow after mixing H_2O_2 and wild-type MnSOD. Scans shown were recorded at (from top to bottom) 2, 34, 82, 130, 226, 514, and 4800 ms after mixing. The solution after mixing contained 0.25 mM wild-type MnSOD, 25 mM H_2O_2, 20 mM KH_2PO_4 buffer at pH 7.8, 50 μM EDTA, and measurements were made at 25 °C. Inset: (1) The spectrum of wild-type MnSOD under the above conditions without the addition of H_2O_2; (2) the spectrum of wild-type MnSOD containing a 50-fold molar excess of azide ion.

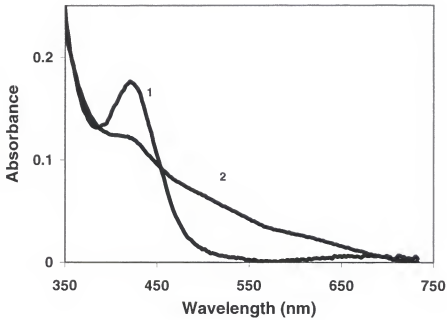

Figure 2-5: Scanning stopped-flow spectra of (1) W161F MnSOD and (2) wild-type MnSOD both 5.2 ms after mixing with 0.95 mM $O_2^{\cdot-}$. The final solution contained 14% dimethyl sulfoxide. The enzyme concentrations used were 0.50 mM in solutions containing 1 mM EDTA and 100 mM Ches at pH 9.1 and 20 °C.

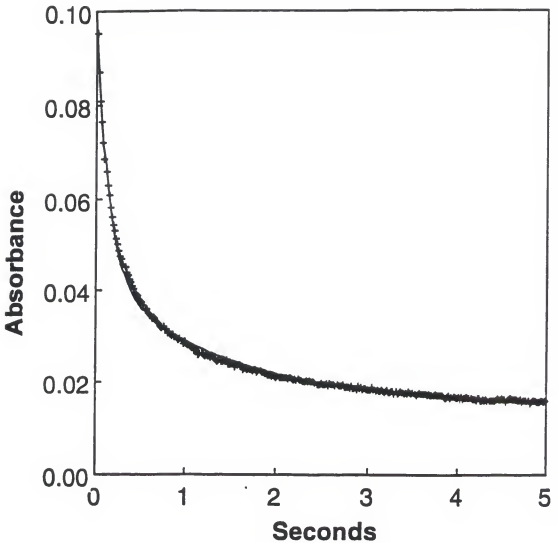

Figure 2-6: The decay of the absorbance at 420 nm after mixing H_2O_2 and wild-type MnSOD via stopped-flow. Solutions after mixing contained 0.25 mM wild-type MnSOD, 25 mM H_2O_2, 20 mM KH_2PO_4 buffer at pH 7.8, 50 μM EDTA. Measurements were taken at 25°C. The solid line is the fit of the data to a second-order process in enzyme concentration with a rate constant of 55.5 ± 0.5 (absorbance units)$^{-1}$s^{-1}. The data appear equally well fit by the sum of two first-order processes with rate constants of 7.0 ± 0.1 s^{-1} and 0.66 ± 0.01 s^{-1}.

CHAPTER 3
STRUCTURAL AND STABILITY STUDIES

Introduction

The metal binding sites of numerous metalloproteins, including Cu/ZnSOD and MnSOD, have been shown to have the metal ligands surrounded by a hydrophobic shell of amino acids. These hydrophobic residues could restrict the flexibility of the direct metal ligands and possibly create a region of low dielectric constant which strengthens the electrostatic interactions of the hydrophilic inner shell of ligands with the metal (Yamashita et al., 1990). For example, carbonic anhydrase, a zinc metalloenzyme, contains a hydrophobic pocket around the active site consisting of Trp, Val, and Leu residues. These residues may also be important for substrate binding (Alexander et al., 1991).

The active site of human MnSOD is surrounded by a series of hydrophobic aromatic residues which are strictly conserved in known sequences of Fe and MnSOD's. This hydrophobic surface is shown in Figure 3-1 and consists of various tryptophans, tyrosines, phenylalanines, and histidines. One of the most prominent residues in the hydrophobic surface is Trp161, which forms one wall of the active site cavity, near the presumed site of substrate entry into the active site. The tryptophan is located 4.68 Å (γ carbon) from the manganese. Due to its size and proximity to the Mn, this residue could have some important structural or catalytic role within the enzyme.

A series of mutations of decreasing hydrophobicity have been made at position W161, including W161F, W161Y, W161H, W161V, W161A. This chapter presents the structure of two of these mutants, W161F and W161A. The W161F mutation is a conservative substitution, while the replacement of the tryptophan with an alanine (W161A) is much less conservative and causes a much greater change in the structure of the active site. The thermal stability of each of the substitutions at position W161 has also been determined; this residue apparently does not provide thermostability.

Materials and Methods

X-Ray Crystallography W161A

Crystal growth and structure determinations for W161A and W161F were carried out in collaboration with Dr. John Tainer at the Scripps Research Institute, LaJolla California. Crystals of W161A human MnSOD were grown from 2-3 M ammonium sulfate in 100 mM imidazole/malate buffer at pH 7.5-8 and belonged to the space group $P6_122$ with a unit cell of 79.6 Å by 79.6 Å by 240.1 Å. A single crystal was used, frozen in a stream of liquid nitrogen and protected by 20% ethylene glycol in the well solution. Data to 2.1 Å resolution was collected at the Stanford Synchotron Radiation Laboratory on beamline 9-1 with 0.77 Å radiation and a MAR-345 scanner and processed using Scalepack and DENZO (Otwinowski and Minor, 1997). Overall, the data was 98.9% complete (100% in the lowest bin) with an R_{sym} of 5.7% (42.7% in the highest resolution bin). The I/σ was 9.8 and in the highest resolution bin it was 4. The protein structure was solved by rigid body refinement of the W161A data against the wild-type structure. Successive rounds of Powell minimizations and B-factor refinement were performed

using CNS (Brunger et al., 1998) and maps ($2F_o$-F_c and F_o-F_c) were fit with the Xfit suite (McRee, 1992), to bring the final R_{cryst} to 24.9 % and R_{free} to 28.9 %.

X-Ray Crystallography-W161F

Rod shaped crystals of W161F MnSOD were grown from solutions consisting of 22 mg/mL protein buffered in 25 mM KH_2PO_4 and 22% poly(ethylene glycol) (PEG) 2000 monomethyl ether. Crystals belong to the orthorhombic crystal form which is homologous to the native human MnSOD crystals with a space group of $P2_12_12$ and unit cell dimensions of a=74.0 Å, b=77.2 Å, and c= 67.8 Å. One flash cooled W161F crystal was mounted under a liquid nitrogen stream and data was collected using the Siemens SRA rotating anode X-ray generator with a MAR-345 area detector. The data were processed using DENZO (Otwinowski and Minor, 1997) and the R_{sym} was 6.4% to 2.3 Å resolution (46.8% for the last bin). The total number of unique reflections was 17730. The structure of W161F mutant was refined with CNS (Brunger et al., 1998) using one dimer of human MnSOD as an initial model. A dimeric W161F model in the asymmetric unit was first rigid-body refined followed by geometry restrained positional refinement. The model was further simulated, annealing refined by heating up to 3000K and gradually cooling down followed by temperature factor refinement in CNS (Brunger et al., 1998). The model was refit to σA weighted $2F_o$-F_c and F_o.F_c maps using Xfit (McRee, 1992). The refinement was completed using a bulk solvent correction in XPLOR (Brunger et al., 1987) with the manganese ion completely unrestrained during the final round of refinement to remove any force field bias. The final model consists of two W161F subunits and 166 solvent molecules with an R-factor of 22.7%.

Differential Scanning Calorimetry

Differential scanning calorimetry experiments were performed in collaboration with Dr. James Lepock at the University of Waterloo, Ontario, Canada. A CSC Nano high sensitivity differential scanning calorimeter was used to obtain all denaturation profiles. Human MnSOD and the W161 mutants at 1.0 mg/ml in 20 mM potassium phosphate buffer (pH 7.8) were degassed under mild vacuum for 5 minutes and immediately scanned at a rate of temperature increase of 1 °C/min. The baseline and change in specific heat (ΔC_p) upon denaturation were corrected by assuming that the baseline immediately preceding the transition and following it were linear, and the baseline under the transition was taken as an average of the two baselines weighted for the fraction of the transition completed. The peaks of the differential scanning calorimetry profile were deconvoluted assuming a reversible, non-two-state model using the software package ORIGIN (Microcal, Inc.). ΔH, ΔS, and T_m for each transition were obtained from the best fits. The T_m values in Table 3-1 are the temperatures at which C_p reached a maximum.

Stopped-flow Spectrophotometry

The effect of the sulfate ion on the catalysis by W161A MnSOD was investigated using stopped flow spectrophotometry (Applied Photophysics, Ltd., SX.18MV) (schematic Figure 2-2). The enzyme was mixed in a sequential manner with a solution of KO_2 in dimethylsulfoxide (DMSO) and 18-crown-6 added to increase the solubility of KO_2 (Valentine et al., 1975; McClune and Fee, 1978). $O_2^{\cdot-}$ in DMSO had been premixed with a solution of 2mM CAPS and 1mM EDTA, pH 11. This premixed solution was diluted (1:10) and then mixed 1:1, following a 500 ms delay for mixing, with the buffered enzyme solution. The final solution after mixing contained 12.5 μM W161A MnSOD, 50

mM Na_2SO_4, 200 mM CHES, 1 mM CAPS, 500 μM EDTA, 5% dimethylsulfoxide, 1mM KO_2, at pH 9.0.

Results

Crystal Structure-W161F

The overall tetrameric structure of W161F closely resembles the conformation of the native human MnSOD (Borgstahl et al., 1992) with an overall root-mean square deviation for Cα's of 0.37 Å. By comparing the detailed wild type and W161F structures, it was found that the side chain of Phe 161 superimposed on that of Trp 161 in the active site. The hydroxyl of Tyr 34 was shifted 1.2 Å in W161F, placing this side chain much closer to the metal in the mutant compared with the wild type (Figure 3-2). The Mn-OH(Tyr 34) distance was 3.9 Å in the mutant and 5.1 Å in the wild type, which places the side chain of Tyr 34 in a more prominent position in the active site of the mutant whereby it may influence catalysis or inhibition. Phe 66 and His 30 were also shifted toward the metal in the mutant. The driving force comes from the smaller side chain of Phe 161 compared to Trp 161. The geometry about the manganese shows that the coordination distances in the mutant are slightly longer, by approximately 0.2 Å, than in the native structure.

Crystal Structure-W161A

Superposition of the structure of human W161A MnSOD with that of the wild-type MnSOD (Borgstahl et al., 1992) showed that the overall structures of these enzymes are nearly identical, and very similar to the mutant W161F (Figures 3-3, 3-4). The root-mean-square deviation between the Cα's of the mutant W161A and wild type is 0.17 Å. The positions of the four amino-acid ligands of the manganese (His 26, 74, 163, Asp 159)

form a strained trigonal bipyramidal coordination in W161A that is very closely superimposable with the wild type (Figure 3-3). It was observed for W161A MnSOD that new water molecules fill the cavity created when this active-site residue is replaced with Ala. Similar observations of new water molecules in mutant structures were made with human Q143A (Leveque et al., 2000) and Q143N MnSOD (Hsieh et al., 1998). One of the new water molecules in W161A approximates the position of the Nε of W161 in the wild type and forms a hydrogen bond with the manganese-bound water (heavy atom distance 2.9 Å) and also with the side chain of Gln 143 (2.9 Å) (Figure 3-3). The side chain of Gln 143 in W161A forms another hydrogen bond with the manganese-bound water (3.1 Å), but this hydrogen bond is weaker than its counterpart in the wild type (2.9 Å). In the wild type, the side chains of Gln 143 and Tyr 34 are hydrogen bonded and form part of an extended hydrogen bond network that also includes His 30 and Tyr 166 (Borgstahl et al., 1992). In the structure of W161A MnSOD, Gln143 rotates slightly to accommodate the smaller volume of Ala instead of Trp at position 161 placing its Nε within hydrogen bonding distance of the manganese bound solvent molecule, as mentioned above, and about 4.0 Å away from the hydroxyl of Tyr 34 which moves quite significantly from its position in the wild-type enzyme (Figure 3-3). In W161A MnSOD the distance between the amide group of Gln 143 and the hydroxyl of Tyr 34 is too great (4.0 Å) to form a hydrogen bond. Hence, W161A interrupts the hydrogen bond network, as do a number of other active-site mutations reported previously (Y34F ,Guan et al., 1998; Q143A, Leveque et al., 2000; H30N, Ramilo et al., 1999).

In the mutant W161A MnSOD, a single sulfate molecule is bound at the dimer interface formed by crystallographic symmetry in the cavity that remains after removing

W161 (Figure 3-3). Two oxygens of this sulfate molecule approximate the positions of two water molecules in the wild type enzyme. It is bound by hydrogen bonds with Tyr34, His 30, and several water molecules. A shift in Y34 seems to occur in response to the changes in Q143 and to accommodate the sulfate molecule. With the sulfate bound, Y34 has rotated, moving the phenolic oxygen approximately 2.2 Å from its wild-type position and breaking the hydrogen bond with Q143, as mentioned above. For residues more distant from the metal, such as His 30, there is no appreciable difference in side-chain conformation compared with wild type, despite a hydrogen bond (2.8 Å) between the side chain Nδ of His 30 and an oxygen of the sulfate.

The mutant W161F was also crystallized in the presence of sulfate for comparison. Here the sulfate also binds to the same location as in the W161A structure. An overlay of the wild type, W161A, and W161F both with and without sulfate is shown in Figure 3-4.

Differential Scanning Calorimetry

Differential scanning calorimetry was used to determine the thermal stability of the human wild-type MnSOD and variants at position 161 (Table 3-1). Modest changes were found in the main unfolding transition, with W161F being the most stable with a 7.1 °C increase in T_m and W161Y the least stable with a 5.6 °C decrease in T_m compared with wild type. W161F and W161Y differ only by one hydroxyl group, but this structural change results in a 12.7 °C change in T_m, suggesting major changes in hydrogen bonding between these mutant enzymes. All of the mutants at position 161 listed in Table 3-1 have values within 7 °C of the wild-type enzyme at 89 °C. The structural changes observed between the wild-type enzyme and the W161A mutant have almost no effect on thermal stability (Table 3-1). The unfolding transition, which is a

measure of conformational stability, is different from the thermal inactivation temperature which is 70 °C for human wild-type MnSOD and is due to a much smaller conformational change for thermal inactivation than for unfolding (Guan et al., 1998). I attempted to prepare other mutants with replacements at 161, such as W161L; however, these were not stable enough to isolate.

Stopped-flow Spectrophotometry

The effect of the sulfate ion on catalysis by W161A was measured by stopped-flow spectrophotometry. Figure 3-5 shows the effect of 50 mM Na_2SO_4 on the zero-order kinetics of the W161A mutant (12.5 μM). The zero-order rate constants for the averaged traces were similar with a rate constant of $k_0/[E_0]$ of 356 s^{-1} without sulfate and 372 s^{-1} with sulfate at pH 9.0.

Discussion

Differential Scanning Calorimetry

In terms of contributions to stability, the wild-type enzyme and the variants at position 161 showed modest differences (Table 3-1), with changes in the major unfolding transition spanning about 7 °C above and below the value of 89 °C for the wild type. The thermal stability of wild-type and W161A MnSOD are nearly identical for this transition. The replacement of Trp161 with Phe or His stabilizes the enzyme, while the replacement by Tyr results in the smallest value of T_m. The hydroxyl of the Tyr appears to be destabilizing while the phenyl ring at this site is stabilizing. These results are consistent with the hypothesis that Trp161, conserved in the MnSOD's, was not selected to confer thermostability for this major unfolding, but to maintain an active-site environment suitable for catalysis.

Stopped-flow Spectrophotometry

The effect of sulfate ion on the catalysis of W161A MnSOD was investigated via stopped-flow spectrophotometry. The enzyme was crystallized in the presence of ammonium sulfate, and a single sulfate was bound in the active site in the crystal structure. Figure 3-5 shows that the presence of sodium sulfate (up to 50 mM) does not have a significant effect on the zero-order catalysis as evidenced by the similar rate constants of the zero-order region of the catalytic traces with and without sulfate. These data imply that modest concentrations of sulfate during catalysis of MnSOD do not have a significant effect on the kinetics of the zero-order inhibited region. Higher concentrations of sodium sulfate (up to 1 M) were investigated; however there was a significant effect of ionic strength on the uncatalyzed rate. Ammonium sulfate was investigated initially, but the presence ammonium ion also affected the uncatalyzed rate even at low concentrations (50 mM).

X-ray Crystallography-W161F

The position of the side chain of Phe 161 in W161F MnSOD superimposes on that of Trp 161 in the wild type (Figure 3-2); the distance from the α carbon of residue 161 to the manganese is unchanged in the mutant. Moreover, there appear no significant changes in the backbone positions between the mutant and wild type. What has occurred in the mutant is a general tightening of the hydrogen-bonded chain from the metal-bound aqueous ligand to His 30 which is characterized by the shortening of several hydrogen bonds. This occurs in a segment of the hydrogen-bonded scheme that connects many side chains and solvent molecules in the active site. In this particular case, the segment altered

involves Mn-aqueous ligand-Gln143-Tyr34-H_2O-His 30. The distance between the manganese and its aqueous ligand may have changed slightly in W161F, increasing by approximately 0.2 Å in the mutant. The hydrogen bond distance between this metal-bound solvent molecule and the amide of Gln 143 is decreased 0.6 Å in the mutant. It is interesting that there is no change in the hydrogen bonded distance between the side-chain amide of Gln 143 and the hydroxyl of Tyr 34; this hydrogen-bonded pair twist as a unit in the mutant so that the hydroxyl oxygen of Tyr 34 in the mutant is 1.2 Å closer to the metal and the amide of Gln 143 is approximately 0.3 Å closer to the metal. The hydroxyl of Tyr 34 is in turn hydrogen bonded through a single water molecule to the side-chain imidazole of His 30, and this distance is smaller by 0.8 Å in the mutant. These features are summarized in the scheme below in which the changes in distances between side chains and metal bound solvent caused by the replacement Trp 161 → Phe are given.

$$\begin{array}{ccccccc} & +0.2\text{ Å} & & -0.6\text{ Å} & & 0 & \quad -0.8\text{ Å} \\ \text{Mn} & \text{—} & \text{solvent} & \text{—} & \text{Gln143} & \text{—} & \text{Tyr 34} \text{ —} \text{ His 30} \end{array} \qquad (3\text{-}1)$$

It is intriguing that these significant structural changes have relatively small effects on the oxidation of superoxide for the W161F compared with wild type (see Table 4-2, k_1). The bigger change, however, is the ten-fold greater product inhibition in the mutant evident in k_2 which corresponds to the regeneration of Mn^{3+}SOD along the uninhibited catalytic pathway (see Table 4-2, k_2). This mutant, along with all of the Trp161 substitutions, exhibit greatly reduced rates of catalysis along the uninhibited pathway (see Chapter 4). The alterations to the hydrogen bonding network in this mutant suggest that this network is important for the transfer of protons to product hydrogen

peroxide and that changes to the network can cause a slower rate of dissociation of product hydrogen peroxide (see Chapter 4 for the kinetics of inhibition for this mutant).

It may be meaningful that the two most inhibited mutants of human MnSOD studied to date have significant alterations to Tyr 34, specifically W161F, in which the hydroxyl of Tyr 34 is 1.2 Å closer to the metal compared with the wild type, and Y34F. It is known that azide binding to the metal of Mn^{3+}SOD of *T. thermophilus* causes an expansion of the coordination geometry to octahedral with the metal-bound azide hydrogen bonded to the hydroxyl of Tyr 34 (Lah et al., 1995). The similarities between the visible absorption spectrum of MnSOD inhibited by azide and the product inhibited complex have been shown in Chapter 2. Hence, the association of product inhibition with mutation or a change in the orientation of Tyr 34 supports a role for this residue and the hydrogen bonding network in promoting the release of product from MnSOD, perhaps through proton transfer. In *E. coli* FeSOD, the side-chain of Tyr34 has been shown to be responsible for the active site pKa of 8.5, which is eliminated in the Y34F substitution. This data supports the involvement of Tyr34 as a possible proton donor to product hydrogen peroxide during the catalysis.

X-Ray Crystallography-W161A

As shown in Figure 3-3, the replacement of Trp161 with Ala caused significant variations in the conformations of the side chains of Gln143 and Tyr34, the two side chains of an extensive hydrogen bond network closest to the metal-bound water (this network includes: the aqueous ligand of Mn, Gln143, Tyr34, His30, and Tyr166) (Borgstahl et al., 1992). To understand more fully this effect, I have compared the structures in this region for different variants of human MnSOD. Figure 3-4 compares the structure of wild-type MnSOD with that of W161A and W161F crystallized in the

presence and absence of sulfate. Most apparent from this comparison is the variation in side-chain conformations of Gln143 and Tyr34. It appears that one function of Trp161 is to constrain the orientations of Gln143 and Tyr34 for participation in the hydrogen bond network. In W161A MnSOD, there is no hydrogen bond between Gln143 and Tyr34. This active site structure is important in maintaining the redox potential as well as the maximal velocity of catalysis (Hsieh et al., 1998; Leveque et al., 2000).

Mutations which interrupt the hydrogen bonding network in human MnSOD have also been investigated in our laboratory. A series of mutations have been made at Gln143 including Asn, Ala, Val, Asn, Glu, and His (Hsieh et al., 1998; Leveque et al., 2000). The most striking effect of breaking the hydrogen bonding network at this site is that the resting state of the enzyme is changed from Mn^{3+} to Mn^{2+}, indicating an increase in the redox potential of the metal. These mutants are associated with at least a 160-fold decrease in the value of k_{cat}/K_m. The crystal structure of the Q143A mutant shows the presence of two additional water molecules in the active site which may be influencing the redox potential of the manganese or causing changes within the hydrogen bonding network in the active site.

A series of mutations were made at position His30 (Asn, Ala, Ser, Glu, Lys, and Gln) which is also involved in the hydrogen bonding network of MnSOD (Ramilo et al., 1999). These mutants show less of a decrease in k_{cat}/K_m, compared to the Gln143 mutants, from 6-fold for H30A to larger decreases for the charged substitutions H30E and H30K. These mutants have Mn^{3+} in the resting state, unlike the Gln143 mutants. The crystal structure of the H30N mutant shows that the side-chain of Asn30 does not participate in the hydrogen bonding network of the active site. In addition, mutations

have been made at position 166, Y166F (Ramilo et al., 1999) and at 34, Y34F (Guan et al., 1998). Mutations of these three prominent hydrogen bonding residues (30, 34, 166) led to a similar decrease in k_{cat} (10- to 20-fold), likely resulting from less efficient proton transfer into the active site. Edwards et al. (2001a, 2001b) have made similar substitutions in *E. coli* MnSOD at Tyr34, Gln146 (equivalent to human Gln143), His30, and Tyr174 (equivalent to human Tyr166) showing similar structural features compared with the work from our laboratory.

In conclusion, Trp161 appears to constrain the conformations of residues comprising the hydrogen bonding network of the active site. When this network is interrupted, proton transfer into the active site during catalysis is hindered and activity is reduced.

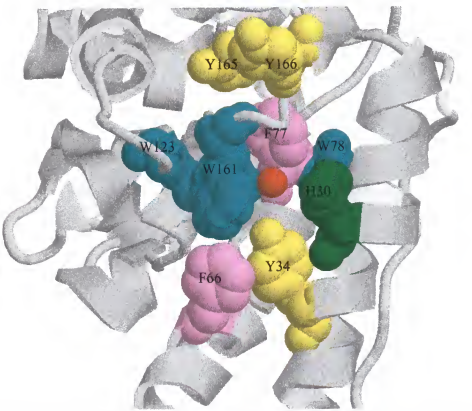

Figure 3-1: The hydrophobic surface of human MnSOD showing the conserved hydrophobic box of residues which surround the active site with tryptophans shown in cyan, phenylalanines in purple, tyrosines in yellow, and histidine in green. For clarity the ligands to the manganese (red) have been omitted.

Table 3-1: Transition Temperatures for the Unfolding of Wild-Type Human MnSOD and Mutants at Position 161

residue at position 161	T_m (°C)
Phe	96.0
His	96.0
Ala	89.8
Trp (wild-type)	88.9
Val	85.1
Tyr	83.3

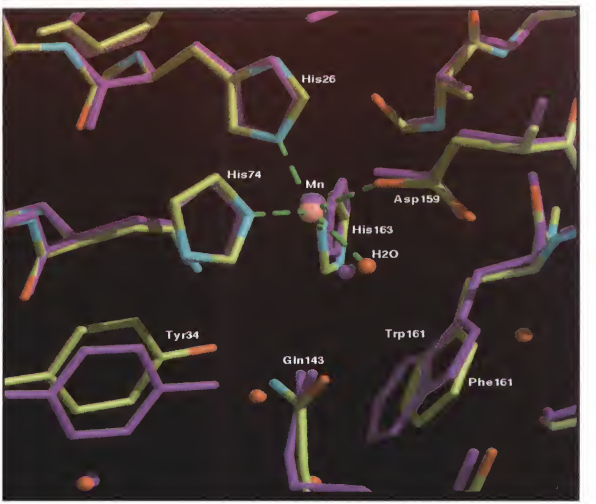

Figure 3-2: Structure of the active site of W161F MnSOD (multicolored) showing the conformation of Phe161 with respect to the Mn and other active site residues from the crystal structure. Wild type structure (purple) is superimposed (Borgstahl et al., 1992)

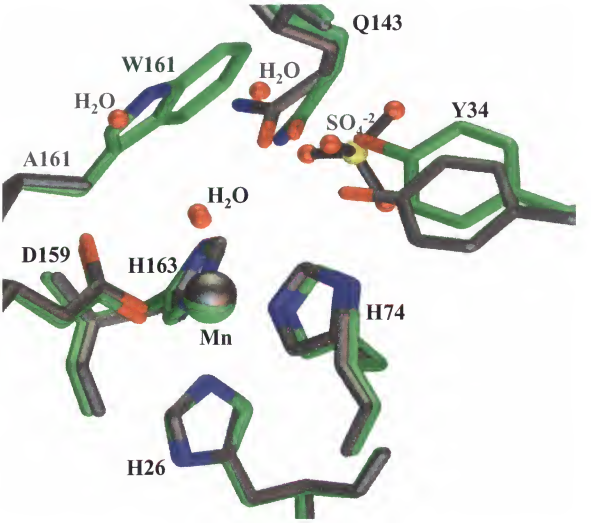

Figure 3-3: Structure of the active site of human W161A MnSOD (gray) superimposed on that of wild-type human MnSOD (green, data from Borgstahl et al., 1992). Sulfate molecule and additional waters labeled in gray correspond to the W161A structure (gray).

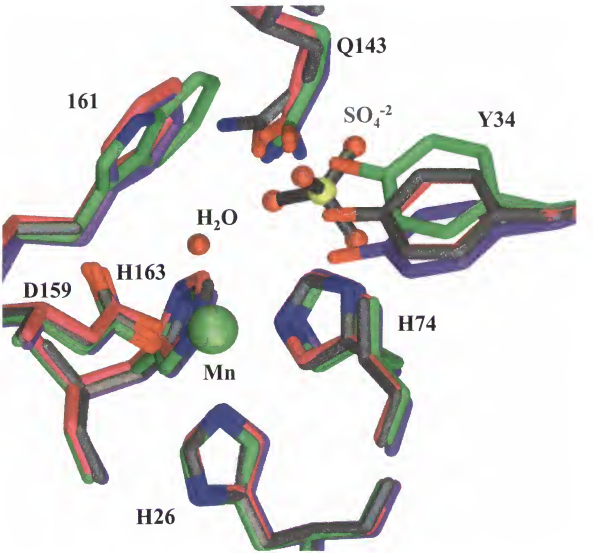

Figure 3-4: Structure of the active site of wild-type human MnSOD (green) superimposed on that of W161F (pink, no sulfate used, from Cabelli et al., 1999); W161F (purple, with sulfate); and W161A (gray with sulfate). The sulfate groups for W161A and W161F are nearly superimposable, and only the W161A is shown for clarity.

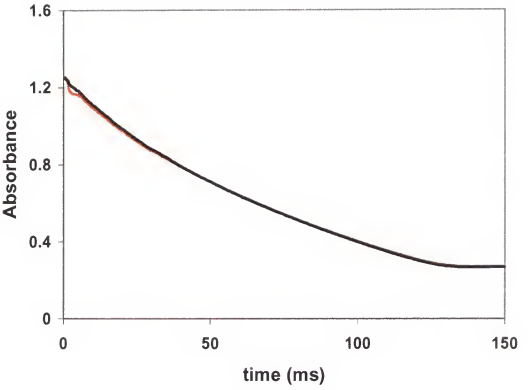

Figure 3-5: The effect of sulfate ion on the zero-order kinetics of W161A MnSOD as measured by stopped-flow spectrophotometry . The absorbance of superoxide (250 nm) vs. time in the catalyzed dismutation in the presence and absence of sodium sulfate is shown. Solutions after mixing contained 12.5 μM W161A MnSOD, 200 mM CHES, 1 mM CAPS, 500 μM EDTA, 5% dimethylsulfoxide, 1mM $O_2^{\cdot-}$, at pH 9.0. The black trace represents no SO_4^{-2} and the red trace includes 50 mM Na_2SO_4 after mixing. The zero-order rate constant $k_0/[E_o]$ was 356 s^{-1} without SO_4^{-2} (black trace) and 372 s^{-1} with SO_4^{-2} (red trace).

CHAPTER 4
KINETIC STUDIES OF THE PRODUCT INHIBITED COMPLEX

Introduction

The focus of this chapter is on product inhibition with emphasis on site-specific mutations at Trp161 of human MnSOD, chosen because W161F MnSOD is the most product-inhibited form of MnSOD reported to date (Cabelli et al., 1999). The side chain of Trp 161 forms one hydrophobic side of the active site cavity of MnSOD with the Nε of its indole ring 5.6 Å from the metal (Figure 3-3) (Borgstahl et al., 1992). The replacement of Trp161 with Ala by site-specific mutagenesis caused significant conformational changes of the side chains of Gln143 and Tyr 34 near the active-site, determined from the crystal structure (Chapter 3).

I have estimated the rate constants for formation and dissociation of the product-inhibited complex by direct observation of characteristic visible absorptions for the free, oxidized enzyme and for the inhibited complex formed during catalysis. Catalysis was initiated by production of superoxide by pulse radiolysis. The data emphasize the role of the competition between catalysis and the steps leading to inhibition, with the mutations at 161 decreasing catalysis and promoting inhibition. The structural changes caused by the mutations at position 161 led to surprisingly little change in the rate constant for

formation of the inhibited complex. Solvent hydrogen isotope effects support a mechanism in which formation of this complex, presumably the peroxide dianion bound to the manganese, involves no rate contributing proton transfer; however, the dissociation of the complex requires proton transfer to generate HO_2^- or H_2O_2.

Materials and Methods

Preparation and Purification of Enzymes.

The human MnSOD cDNA [cDNA sequence by Beck et al. (1987)] was amplified by PCR using the oligonucleotides GCA TAT GAA GCA CAG CCT CC and GGA GAT CTC AGC ATA ACG ATC as primers. The plasmid phMNSOD4 (ATCC 59947) containing human MnSOD was subcloned into the TA cloning vector pCRII (Invitrogen Corp.). Four primers were used to generate the mutants W161X (X = A, F, H, V, Y), H30N, and Y34F. The first pair of oligonucleotides was the same for all of the mutants and was used to regenerate the entire coding region: primer 1: 5' C GCT AGT AAT CAT TTC ATG AAG CAC AGC CTC CCC G-3' and primer 2: 5'-CGC CAA AAC AGC CAA GCT TTC ATG CTC GCA G-3'. The second pair of oligonucleotides (designated primers 3 and 4) were complementary internal primers which encoded the mutation of interest (underlined). The primers used were as follows: W161 primer 3: 5'-GGG ATT GAT GTG TGG GAG CAT GCT TAC-3' and primer 4: 5'-GTA AGC ATG CTC CCA CACATCAATCCC-3', H30 primer 3: 5'-CAG CTG CAC CAT TCG AAG CAC CAC GCG GCC TA-3', and primer 4: 5'-TA GGC CGC GTG GTG CTT CGA ATG GTG CAG CTG-3', Y34 primer 3: 5'-C CAC GCG GCC TTC GTT AAC AAC CTG-3', and primer 4: 5'-CAG GTT GTT AAC GAA GGC CGC CGT GG-3'. The 5' half of the coding sequence was amplified using primers 1 and 4, while a second reaction

using primers 2 and 3 generated the 3' half of the MnSOD coding sequence (Figure 2-1). A second round of PCR was performed using the products from the first two reactions (purified by electroelution) as templates with primers 1 and 2. The restriction sites *Bsp*H I and *Pst* I (incorporated into primers 1 and 2, respectively) were used for cloning the PCR products into the expression vector pTrc 99A (Pharmacia Corp.). The *Bsp*H I site, which is located in the N-terminal portion of the protein, was annealed to the compatible cohesive ends of the *Nco* I site in pTrc 99A, regenerating an ATG codon. *Pst* I was used to cut and anneal the C-terminal end of the cDNA to pTrc 99A. DNA sequencing was used to verify the coding sequence including the new mutation. The plasmid was then transformed into the null mutant *Sod A*$^-$*/Sod B*$^-$ *E. coli* (strain QC774) (Carlioz and Touati, 1986), where it expressed human MnSOD as a mature protein tagged with an extra methionine at the amino terminus. The bacterial media included 660 μM $MnCl_2$. Yields of human MnSOD mutant protein were approximately 70 mg protein per 50 g of bacterial pellet.

Mutant human MnSOD enzymes were purified from *E. coli* by utilizing heat treatment (60 ^{o}C), dialysis (against the appropriate buffer with EDTA), and ion exchange chromatography (DE52 and CM52) according to the procedures previously described (Beck et al., 1988; Chapter 2). SDS-polyacrylamide gels were used to visualize the final purity of the samples. The gels showed one intense band around 22 kDa, indicative of the monomer. After extensive dialysis, the metal content of each of the samples was determined by atomic absorption spectroscopy. The manganese concentration was used in all of our calculations as the concentration of active enzyme. Protein concentrations

were determined by the Lowry method; the ratio of manganese concentration to total protein concentration varied from 0.40 for W161V to 1.00 for W161Y.

Pulse Radiolysis

The pulse radiolysis experiments were performed at Brookhaven National Laboratory using a 2 MeV van de Graaff accelerator. A path length of either 2.0 or 6.1 cm was used for all experiments. All UV/vis spectra were measured on a Cary 210 spectrophotometer at 25 °C. Dosimetry was defined with the KSCN dosimeter, assuming that $(SCN)_2^-$ has a G value of 6.13 and a molar absorptivity of 7950 $M^{-1}cm^{-1}$ at 472 nm (Buxton et al., 1988). The measured rate constants are based on manganese concentration from atomic absorption spectroscopy and not on protein concentration. All of the metal present is presumed to be bound in the active site and functioning independently of the other metal centers. Solutions were made in H_2O or D_2O and contained enzyme and 30 mM sodium formate [as a hydroxyl radical scavenger (Schwarz, 1981)], 50μM EDTA, and 2 mM buffer: Mops (pH 6.5- 7.25), Taps (pH 7.5-9.25), or Ches (pH 9.5-10.5). Superoxide radicals (1-30 μM) were formed by exposing aqueous, air saturated solutions to a high dose electron pulse. In these experiments, $O_2^{\cdot-}$ formation is more than 90% complete by the first microsecond after the pulse. The reactions were monitored by spectrophotometrically following changes in the absorbance of superoxide (Rabani, 1969) or enzyme (Cabelli et al., 1999).

Pulse radiolysis of an oxygen containing aqueous solution generates superoxide radicals by the following reactions (Fridovich, 1986):

$$H_2O \rightarrow OH^{\cdot}, e_{aq}^-, H^{\cdot}, H_2, H_2O_2 \qquad (4\text{-}1)$$

$$e_{aq}^- + O_2 \rightarrow O_2^{\cdot-} \qquad k = 2 \times 10^{10}\ M^{-1}s^{-1} \qquad (4\text{-}2)$$

$$H^{\cdot} + O_2 \rightarrow HO_2 \qquad k = 2 \times 10^{10}\ M^{-1}s^{-1} \qquad (4\text{-}3)$$

The addition of sodium formate doubles the level of $O_2^{\cdot-}$ generated by eliminating $OH^{\cdot}$:

$$HCOO^- + OH^{\cdot} \rightarrow COO^{\cdot-} + H_2O \quad (4\text{-}4)$$

$$COO^{\cdot-} + O_2 \rightarrow CO_2 + O_2^{\cdot-} \quad (4\text{-}5)$$

Solvent hydrogen isotope effects (SHIE) were determined by measuring the ratio of rate constants (under the same conditions) in H_2O and D_2O (>0.98 atom fraction deuterium). Uncorrected pH meter readings are reported. This relies on the fact that the correction of a pH meter reading in 100% D_2O is approximately offset by the change in ionization constant of nearly all acids with values of pKa within the pH range of this study (Schowen and Schowen, 1982). Kinetic solvent isotope effects for the catalyzed dismutation of superoxide were measured at pH 8.2, a value for which measured kinetic constants show no or very little change with small variations in pH.

Results

Observation of the Absorbance of Superoxide

Superoxide was rapidly created by pulse radiolysis (~1μs) in solutions containing dissolved oxygen. The decrease in the absorption of superoxide was followed at 260 nm as a function of time to measure the rate for catalytic disappearance of superoxide in the presence of wild-type MnSOD and mutants. At 3.3 μM initial concentration of $O_2^{\cdot-}$, the decay of superoxide catalyzed by 1 μM W161A MnSOD appeared as a predominantly first-order process; at 17.1 μM initial concentration of $O_2^{\cdot-}$, there was a predominant contribution of a zero-order component (Figure 4-1). This behavior at the higher superoxide concentration is similar to that described for human wild-type MnSOD (Hsu

et al., 1996) and attributed to a product inhibition as seen in bacterial MnSODs (McAdam et al., 1977; Bull et al., 1991).

To fit kinetic data for catalysis by MnSOD from *Bacillus stearothermophilus*, McAdam et al. (1977) proposed a simplified mechanism (eqs 4-3 to 4-6) in which individual steps are considered irreversible, justified in part by the favorable equilibrium constants associated with eqs 4-6 and 4-7. Eqs 4-8 and 4-9 represent the formation and dissociation of the product inhibited complex.

$$\text{Enz-Mn}^{3+} + O_2^{\cdot-} \xrightarrow{k_1} \text{Enz-Mn}^{2+} + O_2 \qquad (4\text{-}6)$$

$$\text{Enz-Mn}^{2+} + O_2^{\cdot-} + 2H^+ \xrightarrow{k_2} \text{Enz-Mn}^{3+} + H_2O_2 \qquad (4\text{-}7)$$

$$\text{Enz-Mn}^{2+} + O_2^{\cdot-} \xrightarrow{k_3} \text{Enz-Mn}^{3+}\text{-X} \qquad (4\text{-}8)$$

$$\text{Enz-Mn}^{3+}\text{-X} + 2H^+ \xrightarrow{k_4} \text{Enz-Mn}^{3+} + H_2O_2 \qquad (4\text{-}9)$$

The advantage of this scheme for this analysis is that it simplifies the catalytic cycle of eqs 4-6 and 4-7 while emphasizing the formation and dissociation of the inhibited complex Enz-Mn^{3+}-X in eqs 4-8 and 4-9. Further implications of this scheme appear in the Discussion of this chapter.

Progress curves such as shown in Figure 4-1 were analyzed by fitting to the data this simplified model of catalysis eqs 4-6 to 4-9 and the known second-order rates of the uncatalyzed dismutation. I used two fitting programs, PRKIN (Schwarz, unpublished) and FITSIM (Zimmerle and Frieden, 1989), which are based on the numerical solution of the simultaneous kinetic equations; both gave the same results. In order to reduce the range of solutions that fit the data such as shown in Figure 4-2, k_3 and k_4 were fixed at the

values shown in Table 4-1 determined, as described below, by direct observation of the characteristic absorbances of the oxidized enzyme and inhibited complex; the fitting programs were then used to obtain the values of k_1 and k_2 . The values of k_2 were small compared with k_1 and k_3 for catalysis by W161A and W161F and allowed me to determine only an upper limit for k_2 (Table 4-2). Because of the similar values of k_2 and k_3 for wild-type MnSOD, I was not able to differentiate these rate constants, and the value represented in Table 4-2 is the sum $k_2 + k_3$. Table 4-2 also gives the values of the zero-order rate constant $k_0/[E_0]$ determined by a fit of data such as shown in Figure 4-1 including a zero-order decay of $O_2^{\cdot-}$ observed at 260 nm.

Observation of the Absorbance of Free and Inhibited Enzyme.

The rate constants k_3 and k_4 that measure the formation and dissociation of the product inhibited complex (eqs 4-5 and 4-6) were determined from the absorption maxima of MnSOD and mutants and their inhibited complexes. The free enzyme W161A Mn^{3+}SOD is characterized by an absorption at 480 nm (Figure 4-2, inset) ($\varepsilon_{480} = 600\ M^{-1}cm^{-1}$ for human MnSOD) (Chapter 2); in the reduced state, MnSOD has only a very small visible absorption (ε_{420} , $\varepsilon_{480} < 50\ M^{-1}cm^{-1}$). The inhibited complex is characterized by a significant absorption at 420 nm shown in the inset of Figure 4-2 for W161A MnSOD ($\varepsilon_{420} = 500\ M^{-1}cm^{-1}$ for human MnSOD)(Chapter 2). W161A MnSOD was reduced with H_2O_2 before single turnover experiments in which $O_2^{\cdot-}$ was generated by pulse radiolysis. Figure 4-2 shows typical data for the first-order increase in absorption at 420 nm as the inhibited complex accumulated. Estimation of the concentration of inhibited complex at the plateau, based on ε_{420} given above, shows all of the $O_2^{\cdot-}$ introduced by pulse radiolysis had been converted to the inhibited form of the enzyme. Since I started with the reduced enzyme, I did not observe the pathway described by eq 4-

6. I have found that for W161A and W161F MnSOD, k_2 is much less than k_3 (compare Tables 4-1 and 4-2). Hence, the increase at 420 nm effectively represents k_3, with little contribution from k_2 of eq 4-7. Values of k_3 were determined in this manner for a series of mutants at position 161 and are presented in Table 4-1 along with a comparison with values determined for H30N and Y34F MnSOD. The data of Table 4-1 demonstrate a surprisingly small variation in k_3 among these active-site mutants.

In an extension of the same experiment, Figure 4-3 shows the first-order increase in the 480 nm absorption due to the decay of the inhibited complex (eq 4-9). This demonstrates, under our conditions, the long separation in time between the formation of inhibited complex, complete by 0.4 ms (Figure 4-2), and its decay, complete in 10 ms (Figure 4-3). The increase at 480 nm, characteristic of the emergence of the oxidized enzyme (Figure 4-3), is mirrored by the decrease at 420 nm (Figure 4-3 inset); overlap of the spectra of W161A Mn^{3+}SOD and the inhibited form at 420 nm makes the magnitude of the change at 420 nm less than at 480 nm (Figure 4-3, inset). A value of $k_4 = 180 \pm 20$ s^{-1} was obtained by a first-order fit to the increase at 480 nm (Figure 4-3); the first-order rate constant from a fit to the decay of the inhibited form at 420 nm (Figure 4-3, inset) was in agreement at $k_4 = 150 \pm 20$ s^{-1}. These values are given in Table 4-1.

Among the mutants of Table 4-1 there is a greater variation in k_4, at most 15-fold, than I observed for k_3. Two mutants noted in previous reports to be particularly inhibited, W161F (Cabelli et al., 1999) and Y34F MnSOD (Guan et al., 1998), have the smallest values of k_4 which are decreased two- to three-fold compared with wild type.

Inhibition pH Profiles

The pH profile of k_3 for W161A MnSOD and $k_2 + k_3$ for wild type were found to have a significant pH dependence above pH 9.0 for the wild type and above pH 8.0 for the W161A mutant (Figure 4-4). The pH profile for W161A could be fit to a single ionization with pKa = 9.2 ± 0.1. The rate constant k_4 for the dissociation of inhibited complex with wild-type enzyme was independent of pH over the range of pH shown in Figure 4-5 with k_4 = 110 ± 10 s-1; however, the W161A mutant showed a significant pH dependence of k_4 with a pKa value of 7.4 ± 0.1 (Figure 4-5).

Solvent Hydrogen Isotope Effects

The solvent hydrogen isotope effects (SHIE) determined for k_3 and k_4 show uniform behavior for wild-type MnSOD and the mutants at position 161 as well as for Y34F MnSOD (Table 4-1). That is, the SHIE on k_3 is unity and that on k_4 is near 2 (Table 4-1). The SHIE for catalysis by H30N are similar within experimental error, but show a somewhat increased SHIE for k_3 (Table 4-1).

Discussion

Kinetics of Position 161 Mutants

I have carried out kinetic measurements of superoxide dismutation catalyzed by series of site-specific mutants at Trp161 of human MnSOD. My emphasis was to elucidate the steps involved in product inhibition during catalysis, and this site was chosen because previous work had demonstrated that the mutant in which Trp161 is replaced by Phe is very product inhibited compared with wild type (Cabelli et al., 1999).

The impact on catalysis of the significant structural changes made at position 161 were investigated by pulse radiolysis in single turnover experiments and analyzed by a

simplified mechanism for catalysis, eqs 4-6 to 4-9. The most significant effect of the replacement of Trp161 with either Phe or Ala is the decrease by at least two orders of magnitude in k_2, accompanied also by substantial although smaller decreases in k_1 (Table 4-2). In previous work, Hsieh et al. (1998) showed changes in the position of the amide group of Gln143 through mutation to Asn and introduction of a new water molecule in Q143N MnSOD resulted in a significant increase in the redox potential of the active site. This suggests that in W161A MnSOD the changes at position 161 and the change in conformation of Gln143 allowing introduction of new water molecules have also altered the redox potential at the active site. The superoxide dismutases have their redox potentials tuned to be between those of the catalyzed half reactions of superoxide oxidation and reduction (Holm et al., 1996; Vance and Miller, 1998), and the data suggest that replacements at position 161 have altered the redox properties of the active site. Any mutation that significantly alters the redox potential of the enzyme out of this range will have a decreased rate of catalysis. W161A and W161F MnSOD are able to oxidize $O_2^{\cdot-}$ with values of k_1 reduced twenty-fold for W161A and five-fold for W161F (Table 4-2), but the values of k_2 for catalytic reduction of superoxide by these mutants were smaller by at least two orders of magnitude.

Competition Between the Inhibited and Uninhibited Pathways

In the wild-type human MnSOD, k_2 and k_3 appear to be of similar magnitude. That is, there is evidence for a competition between these two pathways resulting in an intermediate extent of product inhibition, intermediate between the extensively inhibited W161F and the slightly inhibited H30N mutants (Ramilo et al., 1999). The result is a degree of product inhibition in wild type described in previous reports as occurring on average after several cycles of oxidation and reduction of the uninhibited pathway of eqs

4-6 and 4-7 (Bull et al., 1991; Hsu et al., 1996). However, with W161F the pathway very much favors eq 4-8 leading into the inhibited state. This was a conclusion based on pulse radiolysis data for W161F MnSOD which showed no catalytic cycles occurred but rather showed a pathway that led directly to the inhibited complex.

The significant product inhibition for the position 161 mutants cannot be attributed to any single step, but is a complex process represented by decreases in all of the rate constants for the simplified mechanism of eqs 4-6 to 4-9. However among these, the very low values of k_2 by orders of magnitude compared with wild type appear particularly significant. By decreasing k_2, the presence of Ala161 or Phe161 has favored the formation of the inhibited pathway. That is, the replacement of Trp161 with Ala or Phe has altered the gating between the pathways of catalysis (eqs 4-6 and 4-7) and inhibition (eqs 4-8 and 4-9). Although k_2 is decreased greatly in the position 161 variants, the values of k_3 and k_4 are altered to a much smaller extent (Table 4-1). Hence, the formation (k_3) and dissociation (k_4) of this inhibited complex are not as sensitive to these changes in the active site as is k_2. No correlations were found between the hydrophobicity at position 161 and the values of k_3 and k_4.

Solvent Hydrogen Isotope Effects

The values of the solvent hydrogen isotope effect (SHIE) give a rather consistent picture for all of the position 161 variants shown in Table 4-1. That is, the SHIE on k_3 was unity, indicating no change in covalent binding to hydrogen in a rate-contributing step that leads to formation of the inhibited complex. But there was a SHIE near 2 on k_4 for wild-type MnSOD and all of the mutants of Table 4-1, consistent with a primary proton transfer in the dissociation of the inhibited complex. Overall, the SHIE data are consistent with the formation of a peroxo complex of the metal which occurs with no

rate-contributing proton transfer. It is intriguing that the very significant alterations caused by the replacement of Trp 161 with Ala including the altered conformations of active-site residues Gln143 and Tyr34 have only minor effects on the rate constant for formation of the product inhibited complex k_3 (Table 4-1). This suggests that the formation of this complex is to a considerable extent a function of the metal. However, it is a proton transfer step (or steps) which appears to determine the lifetime of this complex, determined by k_4 of eq 4-9.

Proposals for the formation of the inhibited complex are reviewed by Cabelli et al. (2000). Changes in the visible absorption spectrum of the enzyme in the inhibited state suggest an inner sphere coordination of a form of product peroxide (Bull et al., 1991; Chapter 2). The SHIE of unity on k_3 emphasizes that this complex forms without rate-contributing proton transfer, consistent with an inner-sphere complex of peroxide dianion O_2^{2-} with manganese, possibly a side-on peroxo complex as suggested by Bull et al. (1991). A prominent theme of previous considerations of this catalysis is that a role for the hydrogen bond network in the active site is to support proton transfer to form the hydroperoxide anion HO_2^- or H_2O_2 (Sorkin et al., 1997; Hsieh et al., 1998; Whittaker and Whittaker, 1997). Replacement of Trp161 or Tyr34 with subsequent changes in active-site conformations does have an effect on k_4 with the two most inhibited variants W161F and Y34F MnSOD having the smallest values of k_4 (Table 4-1).

Inhibition pH profiles

The rate constant k_3 for formation of the inhibited complex in W161A MnSOD showed a pH dependence from which I estimate a pK_a of 9.2 ± 0.1 (Figure 4-4), and for wild type the value was 10.3 ± 0.4. The source of this ionization is unknown although it may relate to the pKa of the aqueous ligand of the manganese. Catalysis by wild-type

MnSOD decreases at pH > 9 perhaps due to formation of an additional hydroxyl ligand of the metal (Whittaker and Whittaker, 1997; Lah et al., 1995). The data of Figure 4-5 show that whereas k_4 for wild type is pH independent, k_4 for W161A MnSOD shows a modest pH dependence at pH < 8 (Figure 4-5). It appears that the proton donor to the inhibited complex allowing it to dissociate product is influenced by an ionization with a pKa < 8 in the mutant.

Application of the Simplified Mechanism

The simplified mechanism, eqs 4-6 to 4-9, has allowed me to fit adequately the observed catalyzed decay of $O_2^{\cdot-}$ as well as the formation and decay of the product-inhibited complex. A more extensive model including the reverse reactions has been used to interpret kinetic data for wild-type MnSOD (Bull et al., 1991; Hsu et al., 1996). This more complex scheme was fitted to my kinetic data, which increases considerably the number of fitted variables but affirms the conclusions based on use of the more simplified scheme. For example, application of the more complex scheme estimated that the reverse of eq 4-9 is smaller by about 100-fold than the forward step k_4 for human wild-type MnSOD as well as W161A and W161F mutants. In fact, Chapter 2 shows the observed the characteristic visible absorption pattern of the inhibited complex upon mixing Mn^{3+}SOD and H_2O_2; however, this result required rather large concentrations of H_2O_2 near 25 mM and is certainly not a factor with the much smaller micromolar levels of substrate used in these pulse radiolysis studies.

In conclusion, replacement of the prominent Trp161, which forms a hydrophobic side of the active-site cavity of human MnSOD, has caused significant conformational changes on adjacent residues near the active site, particularly Gln143 and Tyr34 which in wild type participate in a hydrogen bond network believed to support proton transfer

during catalysis. These changes for W161A and W161F MnSOD are associated with a decrease by at least 100-fold in the catalytic reduction of superoxide, which then promotes a competing pathway leading to product inhibition. The rate constant for formation of the product inhibited complex in H_2O and D_2O changes rather little with these significant structural changes in the mutants, indicating that this formation is largely a function of the metal and does not involve a rate-contributing proton transfer. The rate constant for dissociation of the inhibited complex shows a greater variation among these mutants of MnSOD and has a solvent hydrogen isotope effect indicating a rate-contributing proton transfer. These results are consistent with a mechanism in which the inhibited state is a complex of the peroxide dianion O_2^{2-} with the manganese, the dissociation of which as HO_2^- or H_2O_2 is promoted by proton transfer as shown below:

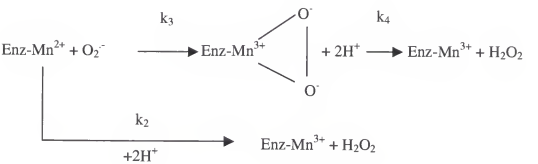

Table 4-1: Rate Constants for the Formation (k_3) and Dissociation (k_4) of the Inhibited Complex and Their Solvent Hydrogen Isotope Effects for Human Wild-type MnSOD and Site-specific Mutants[a]

Enzyme	k_3 ($nM^{-1}s^{-1}$)	k_4 (s^{-1})	$^{D}k_3$ [b]	$^{D}k_4$ [b]
wild type	1.1 ± 0.1 [c]	117 ± 5	1.2 ± 0.2	1.7 ± 0.2
W161A	0.37 ± 0.04	180 ± 20	1.1 ± 0.1	2.3 ± 0.6
W161F	0.46 ± 0.04	33 ± 3	1.0 ± 0.1	2.2 ± 0.2
W161V	0.27 ± 0.01	265 ± 16	1.2 ± 0.1	2.0 ± 0.3
W161Y	0.20 ± 0.01	130 ± 10	1.2 ± 0.1	1.9 ± 0.2
W161H	0.29 ± 0.03	136 ± 7	1.1 ± 0.1	1.8 ± 0.3
Y34F	0.49 ± 0.09	56 ± 4	1.1 ± 0.1	2.0 ± 0.2
H30N	0.68 ± 0.02	500 ± 130	1.5 ±0.1	1.7 ± 0.5

[a] Measured at pH 8.2 and 25 °C with other conditions as described in the legend to Figure 4-2.

[b] $^{D}k_3$ is the solvent hydrogen isotope effect on this constant, $(k_3)_{H2O}/(k_3)_{D2O}$. Similarly for $^{D}k_4$.

[c] This value represents $k_2 + k_3$; due to similar magnitudes for k_2 and k_3 I could not determine these constants individually. See text.

Table 4-2: Rate Constants of Eqs 4-6 and 4-7 for Catalysis by Human MnSOD and the Zero-order Rate Constant Resulting from Product Inhibition [a]

Enzyme	k_1 ($nM^{-1}s^{-1}$)	k_2 ($nM^{-1}s^{-1}$)	$k_0/[E_0]$ (s^{-1})
wild-type	1.5 ± 0.1	1.1 ± 0.1 [b]	500
W161F	0.30 ± 0.08	< 0.01	50
W161A	0.08 ± 0.02	< 0.01	450

[a] These values were determined by a fit to the decrease of the superoxide absorbance at 260 nm, such as shown in Figure 4-1, using PRKIN and FITSIM (Zimmerle & Frieden, 1989), both of which gave the same results within the ranges of standard errors indicated. Conditions as described in Figure 4-1. In this fit, k_3 and k_4 were fixed to the values determined directly from the absorbances of enzyme given in Table 4-1. The range of errors indicates the breadth of solutions determined in the fitting programs.
[b] This value represents $k_2 + k_3$; due to similar magnitudes for k_2 and k_3 I could not determine these constants individually. See text.

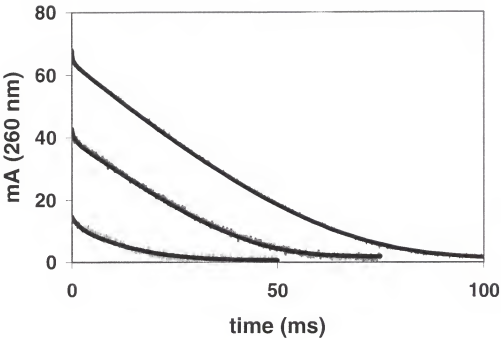

Figure 4-1: Decrease in absorbance of superoxide at 260 nm in the presence of 1 μM W161A MnSOD measured by pulse radiolysis. Solutions contained 30 mM formate, 50 μM EDTA, and 2 mM TAPS at pH 8.2 and 25 °C. Initial concentrations of superoxide were (from top) 17.1, 10.1, and 3.3 μM. The solid lines are a fit of the McAdam mechanism (eqs 4-6 to 4-9) with $k_1 = 8.0 \pm 0.2 \times 10^7\ M^{-1}\ s^{-1}$, $k_2 < 1 \times 10^7\ M^{-1}\ s^{-1}$; $k_3 = 3.8 \pm 0.2 \times 10^8\ M^{-1}\ s^{-1}$, and $k_4 = 140 \pm 11\ s^{-1}$. The value of the zero-order rate constant k_0[E] for the 17.1 μM trace (top) was 450 s-1.

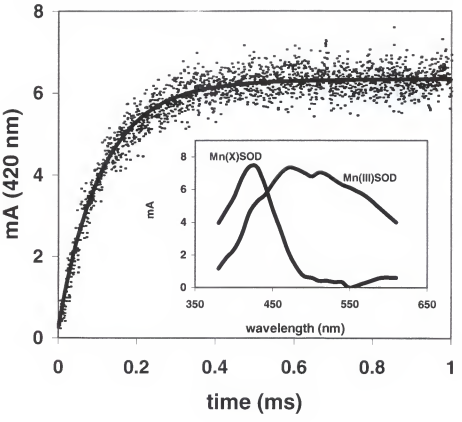

Figure 4-2: Increase in absorbance at 420 nm of 25 μM W161A MnSOD at short times after pulse radiolysis generated an initial concentration of 4.9 μM superoxide. Solutions in H_2O contained 30 mM formate, 50 μM EDTA, 2 mM TAPS at pH 8.2. The enzyme had been reduced prior to the experiment with 200 μM H_2O_2 .The solid line is a fit to a first-order process with the resulting value of k_3 given in Table 4-1. Inset: The visible spectra of W161A Mn^{3+}SOD and the inhibited complex of W161A MnSOD at the same pH.

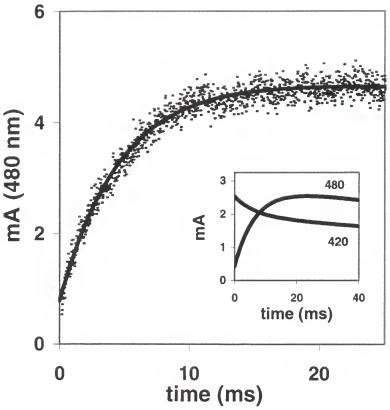

Figure 4-3: Increase in absorbance at 480 nm of 25 μM W161A MnSOD at longer times after pulse radiolysis generated an initial concentration of 4.9 μM superoxide. Conditions as in Figure 4-2. Inset: Changes in absorbance at 480 nm and at 420 nm of 25 μM W161A MnSOD upon exposure to 1.7 μM superoxide. Other conditions as in Figure 4-2. The solid line at 480 nm is a first-order fit with $k_4 = 180 \pm 20\ s^{-1}$. The solid line at 420 nm is first-order fit with $k_4 = 150 \pm 20\ s^{-1}$.

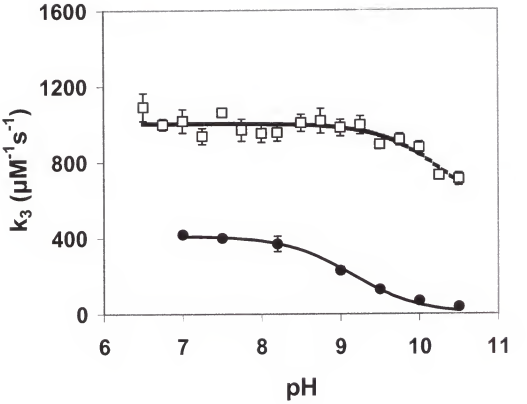

Figure 4-4: The pH profile for the rate constant $k_2 + k_3$ for wild type human MnSOD (□), and k_3 for W161A (●) human MnSOD (eqs 4-7 and 4-8). Solutions at 25 °C in H_2O contained 30 mM formate, 50 μM EDTA, 25 μM enzyme, 200 μM H_2O_2, and 2 mM of one of the following buffers: Mops (pH 6.5-7.25), Taps (pH 7.5-9.25), or Ches (pH 9.5-10.5). Superoxide concentrations were between 1.0 and 2.5 μM. Data are the means and standard deviations of 5 to 10 traces. The data for W161A could be fit to a single ionization with a pK_a value of 9.2 ± 0.1, and the data for wild-type could be fit to a single ionization with a pK_a value of 10.3 ± 0.4.

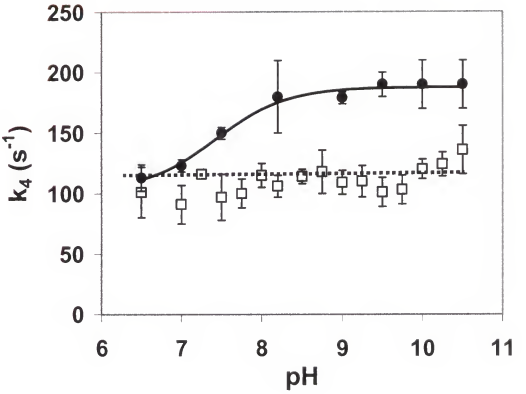

Figure 4-5: The pH profile for the rate constant k_4 (eq 4-9) for wild type human MnSOD (□), and W161A human MnSOD (●). Conditions were the same as in Figure 4-4. The data for W161A could be fit to a single ionization with pK_a 7.4 ± 0.1.

CHAPTER 5
CONCLUDING REMARKS AND FUTURE DIRECTIONS

Conclusions

In this dissertation, I have addressed the role of Trp161 in the active site and its role in product inhibition in MnSOD. My project is the first to identify the inhibited complex of MnSOD as a form of product inhibition. Azide binding studies also give an indication of the structure of the product inhibited complex. Lah et al. (1995) crystallized MnSOD from *Thermus thermophilus* with azide bound and found a six-coordinate species with azide bound to the metal and hydrogen bonded to the hydroxyl of Tyr34. My azide binding studies to MnSOD showed that the spectrum of the inhibited complex and the azide bound form were similar with a maximum absorbance at 420 nm (Chapter 2). These studies suggest that the inhibited complex is a species expanded to six coordinate rather than the five coordinate species seen in the resting Mn^{3+} state. Bull et al. (1991) postulated that the inhibited complex is a side-on peroxo species resulting from the oxidative addition of superoxide to the Mn^{2+} form of the enzyme, based on data from inorganic metal peroxide complexes. This hypothesis is consistent with my data which shows that the formation of this complex is not proton transfer dependent.

My work has also isolated the proton transfer step involved in the decay of the inhibited complex. Interestingly, the two most inhibited mutants we have found in our laboratory (Y34F and W161F) have the slowest rates of dissociation of the inhibited complex (k_4, Chapter 4). Moreover, for the mutants in the Trp161 series there seems to

be a great decrease in the rate of catalysis along the uninhibited pathway (k_2) which could explain the increased levels of inhibition observed in these mutants (Chapter 4). Based on the crystal structure data for the W161A and W161F mutants, it appears that the function of Trp161 and the hydrophobic surface may be to orient the key hydrogen bonding residues involved in proton transfer into the active site and possibly to order solvent within the active site (Chapter 3). Other site-directed mutants replacing residues in the hydrogen bonding network also have large effects upon catalysis and inhibition (Hsieh et al., 1998; Ramilo et al., 1999; Guan et al., 1998; Leveque et al., 2000).

Overall, my data are consistent with the inhibited complex as an expanded six coordinate species which results from the reaction of superoxide with the Mn^{2+} form of the enzyme. The formation of this species is not proton transfer dependent while its decay is, and the isolation of the proton transfer step in inhibition is critical to better understanding the mechanism of inhibition in this enzyme. My data also emphasizes the importance of the positioning of hydrogen bonding residues within the active site to optimize proton transfer during catalysis.

Future Directions

Site-directed Mutagenesis

Mutations of other prominent hydrophobic residues around the active site may be useful in the further investigation of the function of the hydrophobic surface. Trp123 is an interesting candidate because it is slightly further away from the Mn than Trp161 and approaches the active site in a side-on manner. The orientation of this residue is opposite to Trp161 whose π orbitals project into the active site. The possibility of adding more hydrophobicity into the active site is also appealing. Since removal of Trp161 promotes

product inhibition perhaps its addition could ease inhibition. Other hydrophobic residues such as Phe66 could be changed to the more hydrophobic Trp to test this effect; however steric effects could be great due to the large volume of Trp. Double mutants of increased hydrophobicity are also a possibility to determine if there are synergistic effects of hydrophobicity at different sites.

Electron Spin Resonance

Electron spin resonance has been used in our laboratory in collaboration with Dr. Alex Angerhofer in the Chemistry Department (University of Florida). We have used this technique in the past to confirm that one of our mutants, Q143N, had Mn^{2+} in the resting state, compared with Mn^{3+} for the wild-type enzyme. I used ESR in order to determine if the inhibited complex and the azide bound forms of wild-type, H30N, Y34F, and W161F were present in the Mn^{3+} (diamagnetic, no ESR spectrum) or Mn^{2+} (paramagnetic, sextet and doublet of peaks (Hsieh et al., 1998)). In these experiments, I found that the enzyme samples when mixed with hydrogen peroxide and rapidly frozen, did not show the characteristic spectrum of Mn^{2+}. The azide bound enzymes also did not show the characteristic Mn^{2+} spectrum. From these experiments, it was concluded that the inhibited complex and azide bound forms of MnSOD, exist in the diamagnetic Mn^{3+} state. In the future, these experiments could be expanded to a freeze-quench of the enzyme with superoxide to see if similar results are obtained in the dismutation direction.

Redox Potential

Based on my kinetic studies, I suspect that the Trp161 mutants have an increased redox potential (E^o) compared with wild type since these enzymes are hindered in the reduction of superoxide (k_2, Chapter 4). The redox potential (E^o) of the wild-type enzyme is approximately 400 mV (Leveque et al., in press), and since the Trp161

mutants can effectively oxidize superoxide but not reduce it, the redox potential is no longer optimized for both reactions, and the oxidation is favored. One mutation made previously in our laboratory is at position 143, Gln to Asn (Q143N). Based on the wild-type crystal structure, Gln143 is located near the presumed site of substrate entry, and the crystal structure of this mutant shows the presence of an additional water molecule in the active site. The redox potential of the Q143N mutant has been increased significantly from the wild type such that the resting state of the enzyme is no longer Mn^{3+} but rather Mn^{2+} as confirmed by electron spin resonance (Hsieh et al., 1998). The W161A mutant crystal structure also shows the presence of additional water molecules near the active site which may be altering the redox potential of the manganese. I have attempted to measure the redox potential of the W161F and W161A mutants using ferricyanide and ferrocene as mediators. These two mediators have redox potentials close to that of the wild-type enzyme. Mediators are necessary to carry charge because the active site is buried and unable to directly interact with the electrode. I observed no electron exchange between these mediators and the W161F and W161A mutants implying that the redox potential of these enzymes is significantly different from the wild-type enzyme. Future experiments on the redox potential of these enzymes should include various ferrocene derivatives which have higher redox potentials than ferrocene and may be able to exchange electrons with these mutant enzymes. The one obstacle to using the ferrocene derivatives is low solubility in phosphate buffer at pH 7.8, so other conditions must be attempted.

One other possibility with the Trp161 mutants is metal substitution. If the redox potentials of these enzymes are increased relative to wild type, they could show some

activity with Fe in the active site. Fe has the advantage of not being susceptible to product inhibition like the Mn; however it does undergo Fenton chemistry with hydrogen peroxide. Yamakura et al. (1998) showed in *P. gingivalis* FeSOD that Trp159 (human 161) was the residue which was destroyed by oxidation by hydrogen peroxide and resulted in the inactivation of the enzyme. Since the Trp161 mutants lack this key residue, the substituted enzymes may be less susceptible to the effects of the reaction of Fe with hydrogen peroxide and and may be uninhibited as well.

EXAFS

EXAFS (Extended X-ray Absorption Fine Structure) is a very powerful X-ray technique which avoids the use of crystalline enzyme, an advantage over X-ray crystallography. This technique involves measuring modulations in X-ray absorption coefficient around an X-ray absorption edge. By varying the energy of the beam, element specificity is obtained. One advantage of EXAFS is that only atoms within a few angstroms of the atom tuned into are seen. In our site-directed mutants, the changes observed in the crystal structure are often subtle and small, but with EXAFS, changes in metal coordination and bond lengths can be more accurately measured than with crystal structures. This technique was successfully utilized by Stemmler et al. (1997) to examine the binuclear Mn center of the proteins arginase, catalase, and Mn substituted Fe ribonucleotide reductase and hemerythrin. EXAFS could be used to complement the crystal structure data we already have for wild-type and the site-directed mutants of MnSOD. I attempted to perform EXAFS measurements on wild-type and Y34F MnSOD at the Advanced Photon Source (APS) at Argonne National Laboratory. Unfortunately, due to a lack of experience with protein measurements at the APS, these measurements

were unsuccessful. However, Bill Greenleaf in our laboratory has decided to pursue these experiments further.

Another exciting possibility with EXAFS is stopped-flow EXAFS where we could directly investigate the coordination of the inhibited complex with the manganese. This technique holds a great deal of promise for conclusively identifying the structure of the inhibited complex. With stopped-flow EXAFS, we could observe the metal coordination changing from Mn^{3+} to the inhibited complex upon the addition of hydrogen peroxide, or the generation of the inhibited complex from the addition of superoxide to the reduced Mn^{2+} form. Azide binding studies should also be considered to observe the expanded coordination with a substrate/product analog bound.

Resonance Raman Spectroscopy

Resonance Raman spectroscopy is another spectral technique which might complement our crystal structure data and be helpful in determining the coordination and bond lengths of the inhibited complex and the azide bound forms of MnSOD. Resonance Raman spectroscopy has been utilized in the investigation of many manganese containing proteins including: manganese peroxidase (Makino et al., 1986; Mino et al., 1988; Kishi et al., 1996; Sollewijn Gelpke et al., 1999), manganese substituted cytochrome b5 (Gruenke et al., 1997), manganese myoglobin (Yu and Tsubaki, 1980), and manganese containing acid phosphatase (Sugiara et al., 1981).

Proton Coupled Electron Transfer

In the reactions catalyzed by SOD's, both proton transfer and electron transfer are required. Bull et al. (1985) investigated proton uptake by *E. coli* FeSOD upon reduction of the metal and these experiments were extended to the *E. coli* MnSOD by Vance (1999). In both cases, the reduction of the metal was found to be accompanied by proton

uptake. These experiments indicate the presence of a second proton transfer in the catalysis of Fe and MnSOD's. For the reoxidation of the metal, proton transfer is also necessary, as evidenced by the solvent hydrogen isotope effect on the decay of the inhibited complex (Chapter 4). It is unclear if the transfer of protons drives electron transfer or if electron transfer drives proton transfer; however further investigation of the kinetics and the redox potential of the site-directed mutants could show a clear relationship between proton and electron transfer.

REFERENCES

Adelman, R., Saul, R.L., and Ames B.N. (1988) *Proc. Natl. Acad. Sci.* **85**, 2706.

Alexander, R.S., Nair, S.K., and Christianson, D.W. (1991) *Biochemistry* **30**, 11064.

Bannister, J.V., Bannister, W.H., and Rotilio, G. (1987) *CRC Crit. Rev. Biochem.* **22**, 111.

Beck, Y., Oren, R., Amit, B., Levanon, A., Gorecki, M., and Hartman, A. J. (1987) *Nucleic Acids Res.* **15**, 9076.

Beck, Y., Bratfeld, D., Yavin, Z., Levanon, A., Gorecki, M., and Hartman, J.R. (1988) *Biotechnology* **6**, 930.

Beyer, W., Imlay, J., and Fridovich, I. (1991) *Prog. Nucleic Acid Res. Mol. Biol.* **40**, 221.

Borgstahl, G.E.O., Parge, H.E., Hickey, M.J., Beyer, W.F., Hallewell, R.A., and Tainer, J.A. (1992) *Cell* **71**, 107.

Bostantjopoulou, S., Kyriazis, G., Katsarou, Z., Kiosseoglou, G., Kazis, A., and Mentenopoulos, G. (1997) *Funct. Neurol.* **12,** 63.

Brunger, A. T., Kuriyan, J., and Karplus, M. (1987) *Science* **235**, 458.

Brunger, A.T., Adams, P.D., Clore, G.M., DeLano, W.L., Gros, P., Grosse-Kunstleve, R.W., Jiang, J.S., Kuszewski, J., Nilges, M., Pannu, N.S., Read, R.J., Rice, L.M., Simonson, T., and Warren, G.L. (1998) *Acta Cryst.* **D54**, 905.

Bull, C., and Fee, J.A. (1985) *J. Am. Chem. Soc.*, **107**, 3295.

Bull, C., Niederhoffer, E.C., Yoshida, T., and Fee, J.A. (1991) *J. Am. Chem. Soc.* **113**, 4069.

Burgess, J. (1988) Ions in Solution, Ellis Horwood Limited, Chichester, England.

Buxton, G.V., Greenstock, C.L., Helman, L.P., and Ross, A.B. (1988) *J. Phys. Ref. Data* **17**, 678.

Cabelli, D.E., Guan, Y, Leveque, V., Hearn, A.S., Tainer, J.A., Nick, H.S. and Silverman, D.N. (1999) *Biochemistry* **38**, 11686.

Cabelli, D.E., Riley, D., Rodriguez, J.A.A., Valentine, J.S., and Zhu, H. (2000) in Biomimetic Oxidations Catalyzed by Transition Metal Complexes (Meunier, B., Ed.) Chapter 10, Imperial College Press, London, pp 461-508.

Carlioz, A., and Touati, D. (1986) *Embo J.* **5**, 623.

Cerutti, P.A. (1985) *Science* **227**, 373.

Cerutti, P.A., and Trump, B.F. (1991) *Cancer Cells* **3**, 1.

Chance, B., Sies, H., and Boveris, A. (1979) *Physiol. Rev.* **59**. 527.

Choudhury, S.B., Lee, J.-W., Davidson, G., Yim, Y.-I., Bose, K., Sharma, M.L., Kang, S.-O., Cabelli, D.E., and Maroney, M.J. (1999) *Biochemistry* **38**, 3744.

Cooper, J.B., McIntyre, K., Badasso, M.O., Wood, S.P., Zhang, Y., Garbe, T.R., and Young, D. (1995) *J. Mol. Biol.* **246**, 531.

Dougall, W.C., and Nick H.S. (1991) *Endocrinology* **129**, 2376.

Edwards, R. A., Whittaker, M. M., Whittaker, J.W., Baker, E. N., Jameson, G.B. (2001a) *Biochemistry*, **40**, 15.

Edwards, R. A., Whittaker, M. M., Whittaker, J.W., Baker, E. N., Jameson, G.B. (2001b) *Biochemistry*, **40**, 4622.

Fee, J. A., Shapiro, E. R., and Moss, T. H. (1976) J. Biol. Chem. **251**, 6157.

Fridovich, I. (1985) The Harvey lectures, Series, Academic Press, N.Y., **79**, 51.

Fridovich, I. (1986) Adv. Enzymol. Relat. Areas Mol. Biol. **41**, 35.

Gruenke, L.D., Sun, J., Loehr, T.M., and Waskell, L. (1997) *Biochemistry* **36**, 7114.

Guan, Y., Hickey, M.J., Borgstahl, G.E.O., Hallewell, R.A., Lepock, J.R., O'Connor, D., Hsieh, Y, Nick, H.S., Silverman, D.N., and Tainer, J.A. (1998) Biochemistry **37**, 4722.

Gwinner, W., Tisher, C.C., and Nick, H.S. (1995) *Kidney Int.* **48**, 354.

Halliwell, B., Gutteridge, J.M., Blake, D. (1985) *Philos. Trans. R. Soc.* **B311**, 659.

Halliwell, B., and Gutteridge, J.M. (1989) in Free Radicals in Biology and Medicine. Clarendon Press, Oxford, pp 22-408.

Halliwell, B., and Gutteridge, J.M. (1990) *Methods Enzymol.* **186**, 1.

Hassan, H.M. (1988) *Free Radic. Biol. Med.* **5**, 377.

Homma, Y., Tsunoda, M. and Kasai, H. (1994) *Bioch. Biophy. Res. Com.* **203**, 1063.

Housset, B., and Junod, A.P. (1981) *Bull. Eur. Physiopathol. Respir.* **17**, 107.

Hsieh, Y., Guan, Y., Tu, C.K., Bratt, P.J., Angerhofer, A., Lepock, J.R., Hickey, M.J., Tainer, J.A., Nick, H.S., and Silverman, D.N. (1998) *Biochemistry* **37**, 4731.

Hsu, J.-L., Hsieh, Y., Yu, C., O'Connor, D., Nick, H.S. and Silverman, D.N. (1996) *J. Bio. Chem.* **271**, 17687.

Hunter, T., Ikebukuro, K., Bannister, W.H., Bannister, J.V., and Hunter, G.J. (1997) *Biochemistry* **36**, 4925.

Kim, F.J.; Kim, H.P.; Hah, Y.C., and Roe, J.H. (1996) *Eur. J. Biochem.* **241**, 178.

Kishi, K., Kusters-van Someren, M., Mayfield, M.B., Sun, J., Loehr, T.M, and Gold M.H. (1996) *Biochemistry* **35**, 8986.

Krall, J., Bagley, A.C., Mullenbach, G.T., Hallewell, R.A., and Lynch, R.E. (1988) *J. Biol. Chem.* **263**, 1910.

Lah, M.S., Dixon, M.M., Pattridge, K.A., Stallings, W.C., Fee, J.A. and Ludwig, M. L. (1995) *Biochemistry* **34**, 1646.

Lawrence, G.D. and Sawyer, D.T. (1979) *Biochemistry* **18**, 3045.

Leveque, V. J.-P., Stroupe, M.E., Lepock, J.R., Cabelli, D.E., Tainer, J.A., Nick, H.S., and Silverman, D.N. (2000) *Biochemistry* **39**, 7131.

Leveque, V. J.-P., Vance, C.K, Nick, H.S., and Silverman, D.N. (2001) *Biochemistry*, accepted.

Lever, A.B.P. and Gray, H. B. (1978) *Amer. Chem. Soc.* **11**, 348.

Li, Y., Huang, T.T., Carlson, E.J., Melov, S., Ursell, P.C., Olson, J.L., Noble, L.J., Yoshimura, M.P., Berger, C., Chan, P.H., Wallace, D.C., and Epstein, C.J. (1995) *Nature Genetics* **11**, 376.

Makino, R., Uno, T., Nishimura, Y., Iizuka, T., Tsuboi, M., and Ishimura, Y. (1986) *J. Biol. Chem.* **261**, 8376.

Masuda, A., Longo, D.L., Kobayashi, Y., Appella, E., Oppenheim, J.J., and Matsusima, K. (1988) *FASEB J.* **2**, 3087.

McAdam, M.E., Fox, R.A., Lavelle, F., and Fielden, E.M. (1977) *Biochem. J.* **165,** 71.

McClune, G.J. and Fee, J.A. (1978) *Biophys. J.* **24**, 65.

McRee, D.E. (1992) *J. Mol. Graph.* **10**, 44.

Mechler, F., Imre, S., and Dioszeghy, P. (1984) *J. Neurol. Sci.* **63,** 279.

Meier, B., Sehn, A.P., Michel, C., and Saran, M. (1994) *Arch. Biochem. Biophys.* **313**, 296.

Mino, Y., Wariishi, H., Blackburn, N.J., Loehr, T.M., and Gold, M.H. (1988) *J. Biol. Chem.* **263**, 7029.

Murohara, Y., Yui, Y., Hattori, R., and Kawai, C. (1991) *Am. J. Cardiol.* **67**, 765.

Oberley, L.W., Clair, D.K.S., Autor, A.P., and Oberley, T.D. (1987) *Arch. Biochem. Biophys.* **254**, 69.

Oda, T., Akaike, T., Hammamoto, T., Suzuki, F., Hirano, T., and Maeda, H. (1989). *Science* **244**, 974.

Otwinowski, Z. and Minor, W. (1997) *Methods Enzymol.* **276**, 307.

Parker, M.W., and Blake, C.C.F. (1988) *J. Mol. Biol.* **199**, 649.

Rabani, J. and Nielson, S.O. (1969) *J. Phys.Chem.* **73**, 3736.

Ramilo, C.A., Leveque, V., Guan, Y., Lipock, J.R., Tainer, J.A., Nick, H.S. and Silverman, D.N. (1999) *J. Bio. Chem.* **274**, 27711.

Reveillaud, I., Niedzwiecki, A., Bensch, K.G., and Fleming, J.E. (1991) *Mol. Cell. Biol.* **11**, 632.

Richter, C., Park, J., and Ames B.N. (1988) *Proc. Natl. Acad. Sci.* **85**, 6465.

Sawyer, D. T. and Valentine, J. S. (1981) *Accounts of Chem. Res.* **14**, 393.

Schowen, K.B. and Schowen, R. L. (1982) *Methods in Enzymol.* **87**, 551.

Schwarz, H.A. (1981) *J. Chem. Educ.* **58**, 101.

Sollewijn Gelpke, M.D., Moenne-Loccoz, P., Gold M.H. (1999) *Biochemistry* **38**, 11482.

Sorkin, D. L., Duong, D. K., and Miller, A.-F. (1997) *Biochemistry* **36**, 8202.

Sugiura, Y., Kawabe, H., Tanaka, H., Fujimoto S., and Ohara A. (1981) *J. Biol. Chem.* **256**, 10664.

Touati, D. (1988) *Free Radic. Biol. Med.* **5**, 393.

Valentine, J.S., and Curtis, A.B. (1975) *J. Am. Chem. Soc.* **97**, 224.

Vance, C.K. (1999) Thesis dissertation, Johns Hopkins University, Baltimore, Maryland.

Vance, C.K. and Miller, A.-F. (1998) *J. Am. Chem. Soc.* **120**, 461.

Visner, G.A., Chesrown, S.E., Monnier, J., Ryan, U.S., and Nick, H.S. (1992) *Biochem. Biophys. Res. Commun.* **188,** 453.

White, C.W., Avraham, K.B., Shanley, P.F., and Groner, Y. (1991) *J. Clin. Invest.* **87**, 2162.

Whittaker, M.M. and Whittaker, J.W. (1997) *Biochemistry* **36**, 8923.

Wong, G.H.W., Elwell, J.H., Oberley, L.W., and Goedell, D.V. (1989) *Cell* **58**, 923.

Yamakura, F., Rardin, R.L., Petsko, G.A., Ringe, D., Hiraoka, B.Y., Nakayama, K., Fujimura, T., Taka, H., and Murayama, K. (1998) *Eur J. Biochem.* **253**, 49.

Yamashita, M.M., Wesson, L., Eisenman, G., and Eisenberg, D. (1990) *Proc. Natl. Acad. Sci.* **87**, 5648.

Yoritaka, A., Hattori, N., Mori, H., Kato, K., and Mizuno, Y. (1997) *J. Neurol. Sci.* **148,** 181.

Yu, N.T., and Tsubaki, M. (1980) *Biochemistry* **19**, 4647.

Zimmerle, C.T., and Frieden C. (1989) *Biochem. J.* **258,** 381.

Zweier, J.L., Flaherty, J.T., and Weisfeldt, M.L. (1987) *Proc. Natl. Acad. Sci.* **84**, 1404.

BIOGRAPHICAL SKETCH

Amy Hearn was born in Milledgeville, Georgia, on October 18, 1973. She grew up in Coral Springs, Florida. In the fall of 1991, she began her undergraduate studies in the Department of Chemistry at the University of Florida. Following graduation she worked for a year as a polymer chemist, and in the fall of 1996, she enrolled in the Interdisciplinary Program in the Biomedical Sciences Ph.D. program working for Dr. David Silverman in the Pharmacology and Therapeutics Department. Her project focused on product inhibition in human manganese superoxide dismutase. Upon graduation, she will remain in Dr. Silverman's lab while applying for post-doctoral positions at the University of Florida. Her long term goal is to find a position in the pharmaceutical industry.

I certify that I have read this study and that in my opinion it conforms to acceptable standards of scholarly presentation and is fully adequate, in scope and quality, as a dissertation for the degree of Doctor of Philosophy.

David N. Silverman, Chair
Distinguished Professor of Pharmacology and Therapeutics

I certify that I have read this study and that in my opinion it conforms to acceptable standards of scholarly presentation and is fully adequate, in scope and quality, as a dissertation for the degree of Doctor of Philosophy.

William Kem
Professor of Pharmacology and Therapeutics

I certify that I have read this study and that in my opinion it conforms to acceptable standards of scholarly presentation and is fully adequate, in scope and quality, as a dissertation for the degree of Doctor of Philosophy.

Harry S. Nick
Professor of Neuroscience

I certify that I have read this study and that in my opinion it conforms to acceptable standards of scholarly presentation and is fully adequate, in scope and quality, as a dissertation for the degree of Doctor of Philosophy.

Thomas Rowe
Professor of Pharmacology and Therapeutics

I certify that I have read this study and that in my opinion it conforms to acceptable standards of scholarly presentation and is fully adequate, in scope and quality, as a dissertation for the degree of Doctor of Philosophy.

Daniel Purich
Professor of Biochemistry and Molecular Biology

This dissertation was submitted to the Graduate Faculty of the College of Medicine and to the Graduate School and was accepted as partial fulfillment of the requirements for the degree of Doctor of Philosophy.

August 2001

Dean, College of Medicine

Dean, Graduate School